NASA TECHNICAL NOTE

NASA TN D-6093

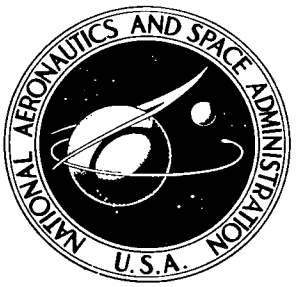

A NOVEL, AXISYMMETRIC, ELECTROSTATIC COLLECTOR FOR LINEAR BEAM MICROWAVE TUBES

by Henry G. Kosmahl

Lewis Research Center

Cleveland, Ohio 44135

NATIONAL AERONAUTICS AND SPACE ADMINISTRATION • WASHINGTON, D. C. • FEBRUARY 1971

1. Report No.	2. Government Accession No.	3. Recipient
NASA TN D-6093		

4. Title and Subtitle: A NOVEL, AXISYMMETRIC, ELECTROSTATIC COLLECTOR FOR LINEAR BEAM MICROWAVE TUBES

5. Report Date: February 1971

6. Performing Organization Code:

7. Author(s): Henry G. Kosmahl

8. Performing Organization Report No.: E-5813

10. Work Unit No.: 164-21

9. Performing Organization Name and Address
Lewis Research Center
National Aeronautics and Space Administration
Cleveland, Ohio 44135

11. Contract or Grant No.:

13. Type of Report and Period Covered: Technical Note

12. Sponsoring Agency Name and Address
National Aeronautics and Space Administration
Washington, D. C. 20546

14. Sponsoring Agency Code:

15. Supplementary Notes:

16. Abstract

A novel, electrostatic depressed collector for microwave tubes is analyzed. The boundary-value problems, space-charge effects, and trajectories are treated accurately. The design eliminates most of the deficiencies of "older" collectors and promises to recover up to 80 percent of the energy of spent beams even in the presence of high axial and radial velocity spread.

17. Key Words (Suggested by Author(s)): Novel depressed collector for microwave tubes

18. Distribution Statement: Unclassified - unlimited

19. Security Classif. (of this report)	20. Security Classif. (of this page)	21. No. of Pages	22. Price*
Unclassified	Unclassified	50	$3.00

*For sale by the National Technical Information Service, Springfield, Virginia 22151

A NOVEL, AXISYMMETRIC, ELECTROSTATIC COLLECTOR FOR LINEAR BEAM MICROWAVE TUBES

by Henry G. Kosmahl

Lewis Research Center

SUMMARY

An analytical model of a novel, axisymmetric, electrostatic depressed collector for linear beam microwave tubes is introduced. The model features schemes for independently effecting the sorting of low- and high-energy electron classes, prevention of backstreaming secondaries and primaries, and a geometry that makes the size of the beam unimportant for the shape of trajectories.

The boundary-value problem is solved by developing a Green's function in elliptical harmonics. The trajectories are derived from Lagrangian equations including accurate space-charge effects. The magnetic boundary-value problem is solved for an ideal shield with an aperture for the exit of the spent beam. The charge conservation is treated for two assumed velocity distributions across the beam: a nearly parallel multivelocity beam of constant current density and a diverging multivelocity beam. Examples of digitally computed electron trajectories are shown. The performance of the collector and the problem of optimizing the overall tube-collector efficiency is discussed.

INTRODUCTION

The residual energy in spent electron beams emerging from the exits of microwave tubes represents not only a loss in efficiency but also an unnecessary heat dissipation burden. The advent of space communication systems with their demands for highest realizable overall efficiencies and, if possible, for the elimination of the cooling problem makes the recovery of this energy mandatory. Since we deal here with kinetic energies of electrons, an obvious approach is to slow down the electrons and collect them on surfaces at the lowest possible potentials. The name "depressed collector" appropriately describes devices fulfilling this purpose.

Depressed collectors have been subject to numerous experimental investigations and

a few simplified and quite superficial analytical treatments since the late fifties. Wolkstein (ref. 1) and Sterzer (ref. 2) pioneered in successfully applying a one- or two-segment depressed collector, respectively, to low-efficiency traveling wave tubes. Their collectors consisted essentially of one or two segments of cylindrical tubings insulated from each other and shielded from the focusing magnetic field. Since in low-power, low-efficiency tubes both the radial and axial velocity spreads are small, a significant improvement factor in efficiency in comparison to "undepressed" operations was achieved. The degree of depression, while being far less than a theoretical maximum, was determined by the onset of backstreaming electrons, either reflected primaries or secondaries. Moreover, since the metallic boundaries of the segments did not coincide with natural equipotential surfaces, strong fringing fields ("lens effects") were formed. It is obvious that the presence of such fringing, strongly curving fields will, in general, prevent the collection of electrons at lowest possible potentials and will also cause the backstreaming of many electrons, not necessarily due to a lack of energy but rather because of unfavorable deflections.

Attempts to improve the overall tube efficiency by collector depression in high-power tubes with large velocity spreads were many, but not much success was achieved with conventional techniques. With a few exceptions, the results were published only in internal reports.

New approaches which eliminate some of the deficiencies of the earlier works were introduced by Sauseng (refs. 3 and 4) and Branch and Mihran (ref. 5) and Neugebauer. An effective method to suppress secondaries and their backstreaming was introduced at Bell Telephone Laboratories, and later at Hughes by Sauseng, by collecting electrons in negative electric fields. To enhance the velocity sorting, Sauseng (ref. 4) employed an asymmetric magnetic deflection. This method, although it is very effective in sorting off-axis as well as on-axis electrons, seems to have a basic deficiency due to unequal action of the magnetic field on electrons parallel and perpendicular to it.

Branch and Mihran (ref. 5) and Neugebauer found the interesting property of electrons deflected by a long symmetric negative spike to "focus" at one point after coming down from the apex of the trajectory.

The approach pursued in the present investigation takes a basic configuration of a sphere with a central cone and a short protruding spike as a flexible geometry to perform three functions effectively at the same time: that is, (1) to velocity-sort the electrons, (2) to slow them down to minimum realizable velocity at collection, and (3) to prevent the backstreaming of secondaries and reflected primaries into the interaction region of the tube.

METHODS OF SOLUTION

The solution of the potential problem is derived in appendix A with the powerful and elegant tool of Green's function.

As shown in figure 1, the cone, the spike, and a part of the spherical surface are assumed to be at the potential $-1.5\ V_o$, the surface adjacent to the injection hole at $V = 0$ and a continuous distribution from $V = 0$ to $-1.5\ V_o$ over the rest of the surface. (All symbols are defined in appendix F.) Here, the cathode is at a potential $-1.0\ V_o$, the tube output at $V = 0$. In the tube considered for future applications, only very few electrons will have energies larger than $1.5\ V_o$. Thus, there will be little interception on the spike and cone. The distribution of the potential between hole and cone on the boundary of the sphere is a variable to be chosen such that sufficient sorting is obtained with the highest possible energy recovery. It is obvious that a purely electrostatic deflection requires some small part of axial energy to be converted into radial components which produce the sorting.

It is apparent from reviewing previous efforts with "conventional" collectors that their failure to perform effectively the first and third required functions limited their usefulness in applications to more efficient tubes. In contrast to this deficiency, an inspection of the equipotential lines and collecting electrodes, as well as of the apertures for the electron passage, shows the effectiveness of the present design to fulfill all requirements. Since the equipotential lines slope upward, the direction of force on electrons is away from the axis of symmetry. Also, the sharp spike produces an indentation in the equipotential lines in the immediate vicinity of the axis. Thus, slight perturbations such as noise, small plasma fluctuations, or residual signals will cause even electrons going straight up to be quickly deflected away from the axis, where they become subject to sorting and collection. These processes are discussed in the section Analytical Results.

Initial Beam Conditions

Any exact calculation of electron trajectories in the collector region, which is treated in appendix B, presupposes a knowledge of the electron vector velocity distribution in the entrance plane as a function of time, that is, for all phases of the full radio-frequency cycle. If azimuthal symmetry is assumed, the problem is reduced to the knowledge of a distribution function $f_i(r, z, \dot{r}, \dot{z}, \dot{\varphi}, t)$ in a six-dimensional phase space, the subscript i designating the initial injection plane. Since presently available nonlinear (large signal) computer programs are one-dimensional, f_i is not yet known. However, from fairly accurate nonlinear three-dimensional calculations (unpublished current

work of this author), it is evident that most electrons enter the collector at angles α_i between 0^o and 15^o at radiofrequency voltage levels from zero to V_o, the degree of deflections being determined almost entirely by the distance from the axis rather than by phase or radiofrequency voltage. Since these calculations were carried out for, among others, a confined flow through a magnetic field of magnitude two to three times the Brillouin field B_B, terminated by an ideal shield, it is obvious that the magnetic deflection largely dominates the problem. Thus, in absence of exact data, a deflection angle proportional to the radial position of the electron may be assumed. Aside from the direction, the magnitude of the velocity is of interest. Especially at high frequencies (e.g., larger than X-band), the beam diameter is so small compared to collector dimensions that the electrons may be considered as coming from a point source, but with an equivalent distribution ranging from about zero to 2 V_o, depending on radiofrequency phase. Another important feature of the beam is its degree of laminarity. The problem is complicated by the number of possible cases, including klystrons and traveling wave tubes (TWT) and solenoid and ppm focusing. In a well-focused, confined-flow klystron beam through a solenoid, good laminarity may be assumed everywhere, except in the output cavity during decelerating fields. In a solenoid-focused, coupled-cavity TWT, the onset of nonlaminarities may begin two or three cavities prior to the output. In ppm-focused tubes, nonlaminar behavior may prevail over the end of the tube due to strong scalloping. Thus, an exact analysis of ppm-focused traveling wave tubes is so complex that efforts toward providing it should be critically evaluated with regard to its importance.

Fortunately, all indications show that the majority of the electrons will be contained within a small angle in all cases except electrostatically focused tubes. Thus, their radial velocities can be reduced, though not eliminated, sufficiently to permit a substantial energy recovery in the collector. Another argument to be accepted is the fact that even if the exact electron distribution were known, no single or simple enough refocusing method would eliminate the radial spread for all electrons at all phases.

Space-Charge Effects

It is appropriate at this time to evaluate qualitatively the effects of space charge on the operation and performance of the collector. Whereas at low frequencies ($f \leq 2$ GHz) the current density at the entrance into the collector is of the order of 1/2 to 3 amperes per square centimeter, this number increases to approximately 40 to 100 amperes per square centimeter at 12 gigahertz, depending on perveance. An examination of the trajectories and equipotential lines obtained for the two frequencies and presented in figures 1, 2, 4, and 3, respectively, demonstrates clearly the highly undesirable effects of high space charge on the trajectories and performance. In the low-frequency design

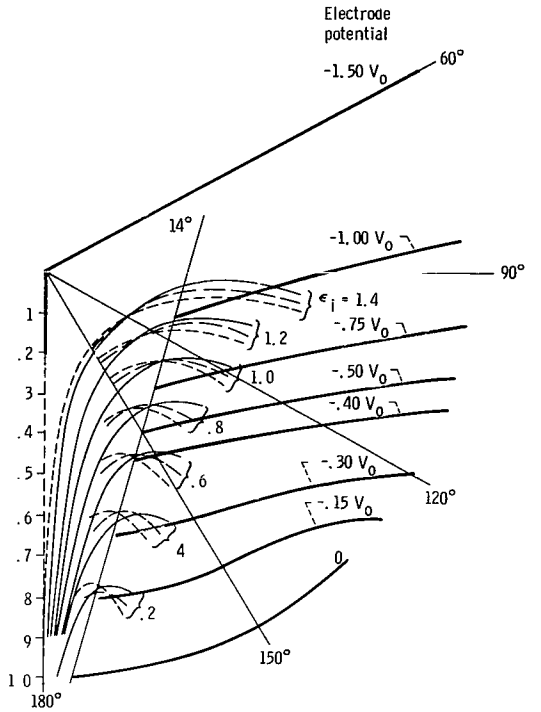

(a) Electron injection radius, $0 < r < 0.6$ centimeter; maximum injection angle, 13°.

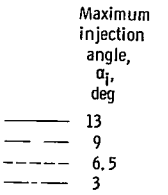

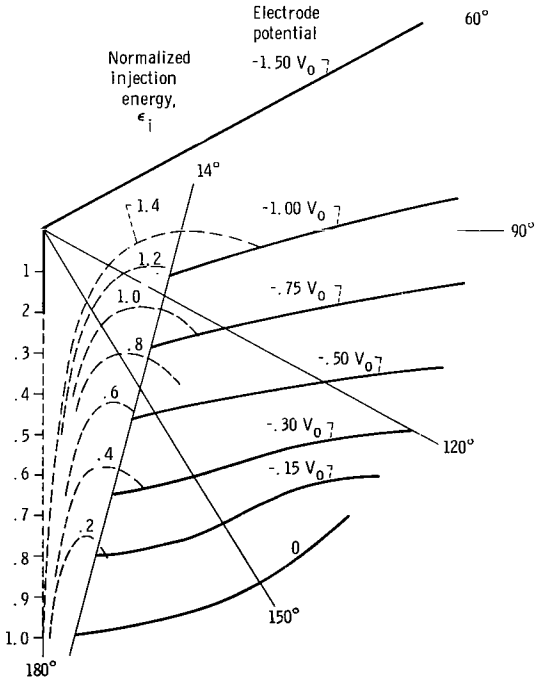

(b) Electron injection radius, $0 < r < 0.3$ centimeter; maximum injection angle, 6.5°.

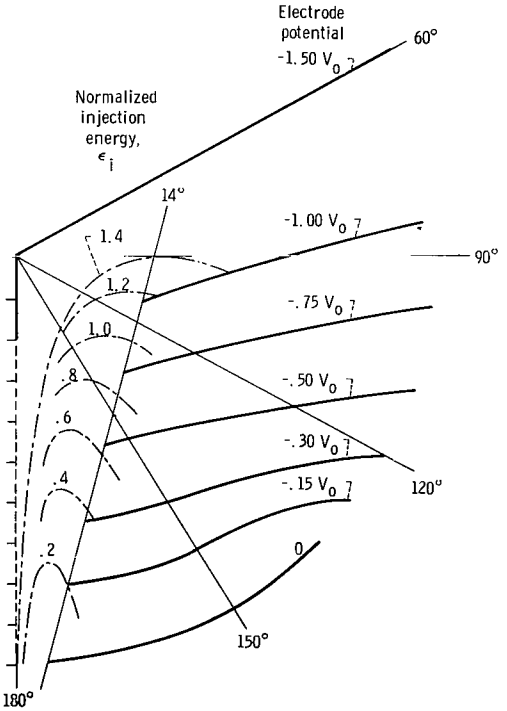

(c) Electron injection radius, $0 < r < 0.3$ centimeter; maximum injection angle, 3°.

Figure 1. - Trajectories and equipotentials for a collector with a 0.2 R long spike. Magnetic field intensity, 0; current density, 0.5 ampere per square centimeter; radius of sphere, 16 centimeters.

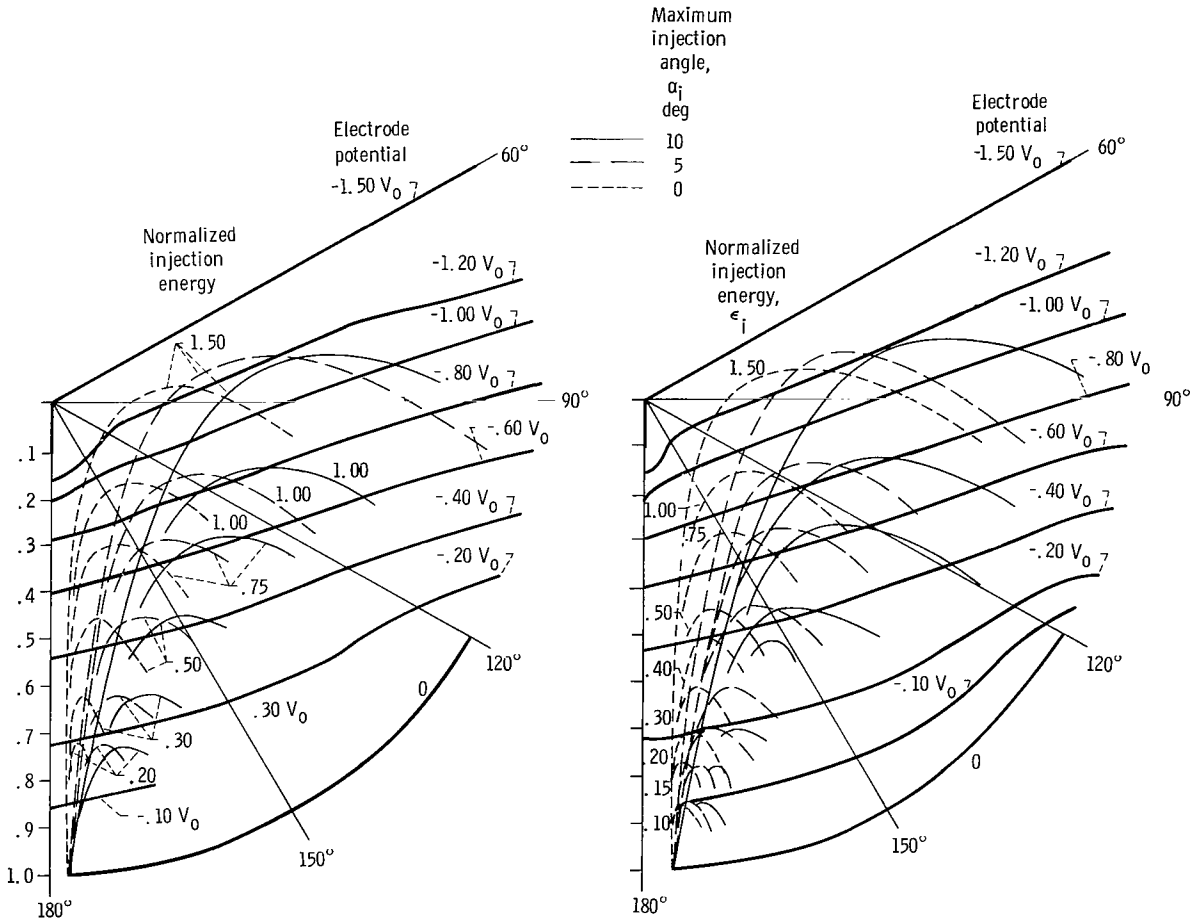

(a) Electron injection radius, 0.4 centimeter.

(b) Electron injection radius, 0.8 centimeter.

Figure 2. - Trajectories and equipotentials for a collector with a 0.1 R long spike. Magnetic field intensity, 0; current density, 0.5 ampere per square centimeter; injection angles, 0°, 5°, 10°.

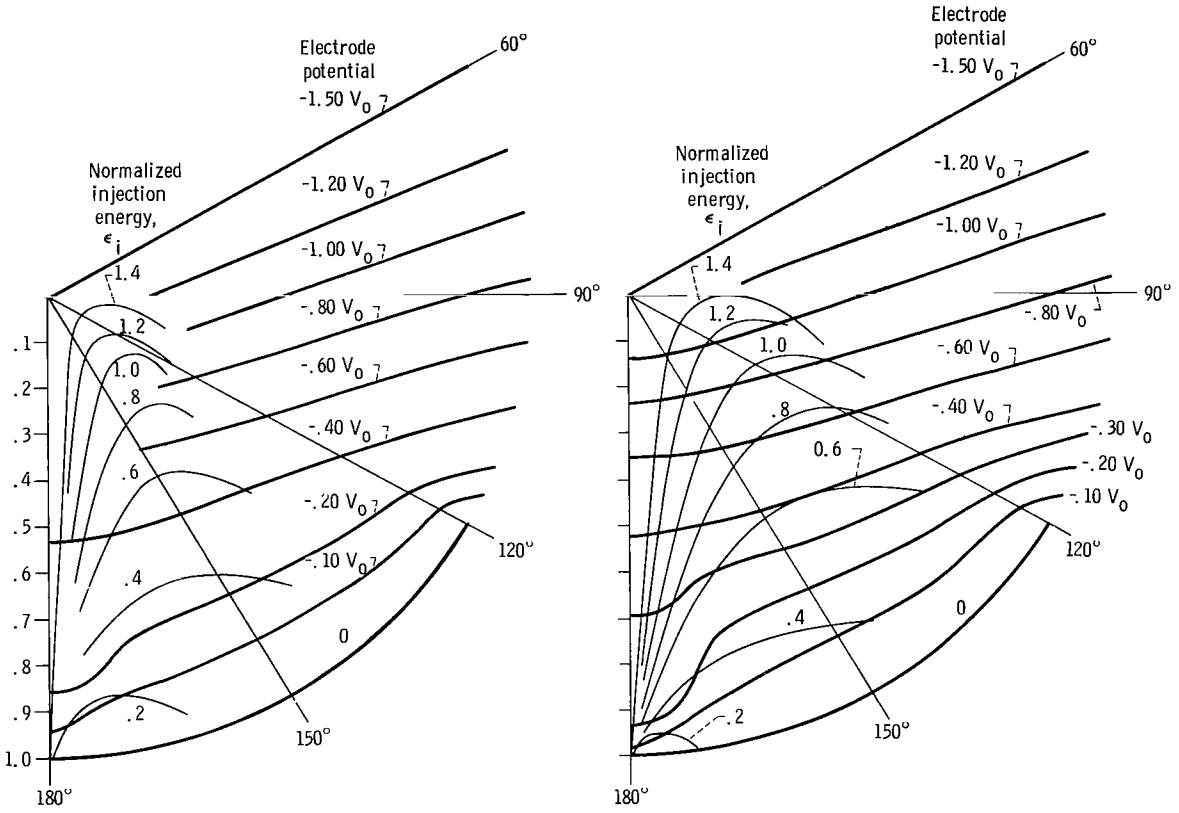

(a) Current density, 30 amperes per square centimeter.

(b) Current density, 90 amperes per square centimeter.

Figure 3. - Trajectories and equipotentials for a collector without a spike. Magnetic field intensity, 0; electron injection angles between 1° and 16°; injection radius, 0.1 centimeter.

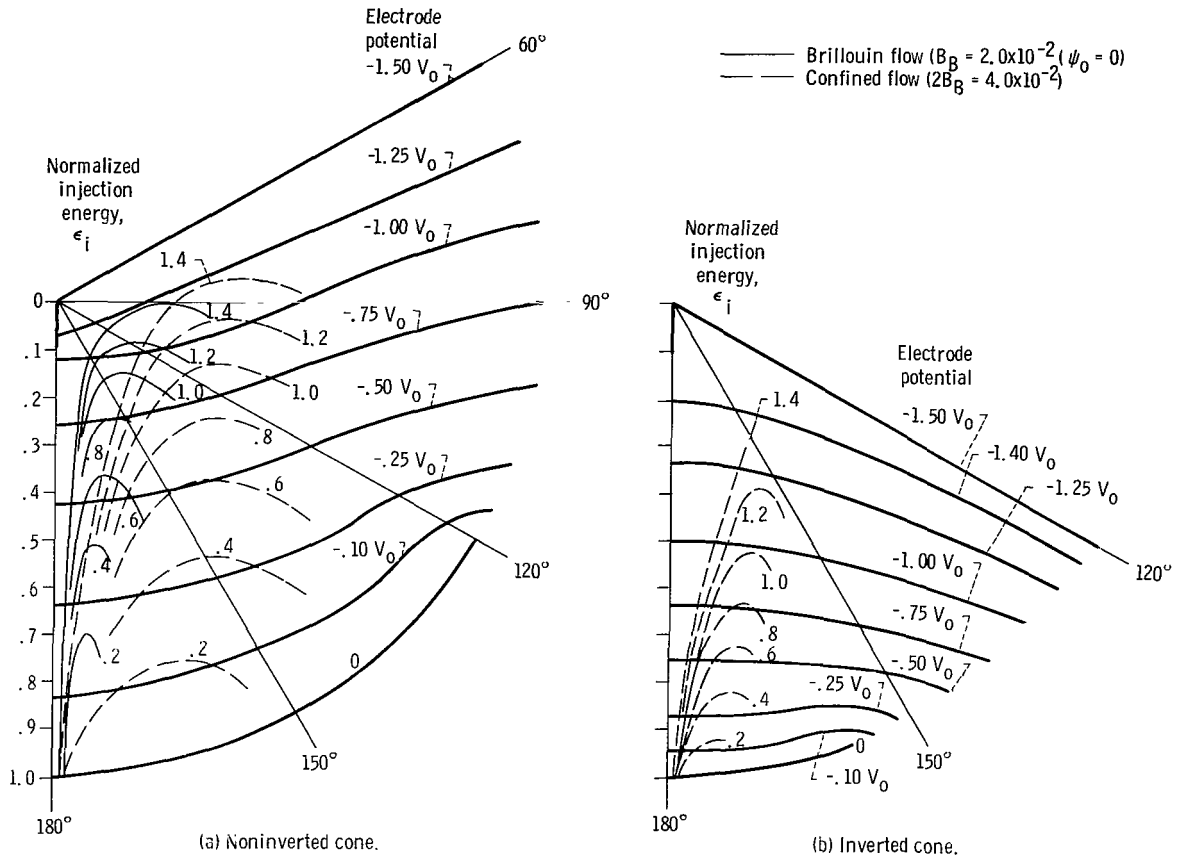

Figure 4. - Trajectories and equipotentials for a magnetically confined flow beam and Brillouin flow. Frequency, 2 gigahertz; current density, 0.5 ampere per square centimeter.

(small space charge) shown in figures 1, 2, and 4, the Poisson solution hardly differs from the Laplace solution; that is, the external fields dominate the potential shape and electron flow. On the other hand, in the high-frequency case (fig. 3), not only are the space-charge fields much stronger (in the vicinity of the injection hole) than the space-charge-free fields produced by external potentials, but there is an acute danger of space charge blocking the flow of electrons and a buildup of a virtual cathode. The deformation and depression of equipotential lines causes an excessive deflection of electrons radially outward, thus decreasing the degree of energy recovery. In addition, the direction of the flow is clearly space-charge dominated, making a planned velocity-sorting very difficult and very sensitive to space-charge fluctuations and possible instabilities. In addition, a refocusing of such high-density beams is not practical. We must, therefore, conclude that a substantial dilution of high current densities down to 1-ampere-per-square-centimeter levels is required if collectors designed for high-frequency tubes are

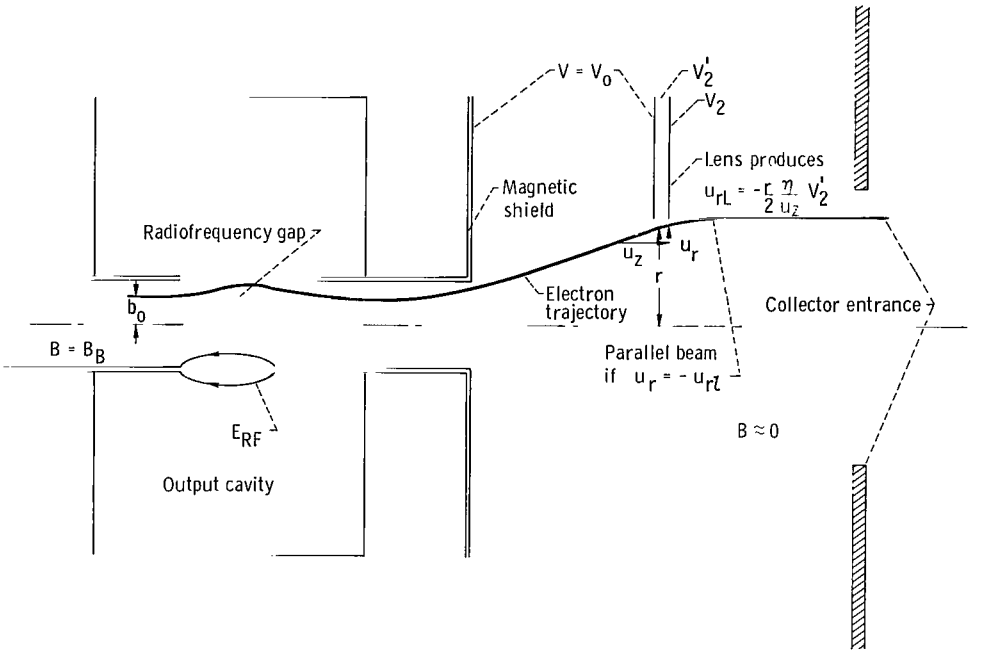

Figure 5. - Refocusing of spent beams with electrostatic lens. Requirement for parallel beams: $u_r = (\eta/2V_2')(r/u_z) = C(r/u_z)$.

to be made feasible and approximately as efficient as low-frequency designs. A possible arrangement to accomplish this task is shown in figure 5 and is discussed in the section Analytical Results. For the case of the highly desirable small space charge in the collector region, even large errors in computing ρ_e will not change the trajectories significantly. This, in turn, permits the application of simplified methods for obtaining an expression for ρ_e. For this reason, a semi-quantitative approximation is made regarding the velocity vector distribution across the beam. This approach is treated in appendix C in connection with the continuity equation.

The leakage of the magnetic focusing field into the collector region through the aperture in the shield is solved in appendix D. An existing axisymmetric expansion of the vector potential is used within the diameter of the solenoid, using the field along the axis. In addition, a solution valid everywhere is derived by transforming the scalar potential, resulting from solving the magnetic-boundary-value problem on the shield and in the aperture from spheroidal oblate coordinates into spherical coordinates.

The relations relating tube efficiency, collector efficiency, and overall efficiency are discussed in the section Analytical Results.

The international system of units is used throughout.

DISCUSSION OF COLLECTOR OPERATION

General Considerations

Consider the computed electron trajectories in figures 1 to 4. They represent the motion of a spent electron beam which, while being axisymmetric, has a wide distribution in energy, radial and axial velocities, and radial distance from the axis at the time of entry into the collector. It is clear, therefore, that the task to collect all electrons which started within a given range of initial kinetic energy at close to zero final energy on the same electrode regardless of angle, radial position, and radial velocity is an impossible proposition for a static arrangement of electrodes. This difficulty can, however, be somewhat mitigated by making the beam radius at entry small compared to the distance the electrons have to travel from injection point to collection point. In this case the electrons appear to be coming from a point source, thus rendering the distribution in radius unimportant. For the range of remaining variables (i.e., the distribution in energy and direction), a compromise must be made such that the impact kinetic energy is a minimum.

Another important design feature is the degree of flexibility in accomplishing the sorting into energy (velocity) classes. Some axisymmetric collectors (ref. 5) use a long, protruding spike as the only sorting (deflecting) element. In the present configuration the sorting is effected separately by a relatively short spike, which acts mainly on the more energetic electrons, and by the potential distribution on the sphere and the cone, which determines mainly the slope of the equipotentials in the vicinity of the entrance. The advantage of this flexibility becomes apparent if particular velocity classes are injected in a preferential direction which requires a different degree of sorting (deflecting force) for different energy classes. For high collector efficiency, only as little radial deflection should be applied as is necessary for steering the electrons of a given energy class to an electrode, where they can be collected with a minimum of total kinetic energy, that is, axial and radial components.

Still another important requirement concerns the prevention of backstreaming of primaries and secondaries. As mentioned earlier, streaming of secondaries may be eliminated entirely if they are generated on the "upper" side of the electrodes facing negative electric fields. The analysis and visual inspection of trajectories shows that a great majority of trajectories are collected on the upper side of the plates (except on the cone and the spike). However, a small fraction of electrons will strike the edge of the underside causing the generated secondaries to stream to the next higher potential electrode. In order to keep the area of the struck edge as small as possible, the electrodes should slope "upward" away from the axis.

As far as the backstreaming of reflected primaries is concerned, the best way of

keeping this effect to a minimum is by designing the diameter of the apertures in the electrodes as small as possible. The limit on the size is dictated by the onset of primaries impinging on the undersides, which prevents energetic electrons from being collected at yet lower potentials. Theoretically speaking, there is, in the axisymmetric configuration discussed herein, no possibility of preventing backstreaming of primaries and secondaries which move down exactly along the axis since there is no radial (deflecting) force along it. However, the number of electrons within a given radius is proportional to r^2, where r is the distance from the axis. Thus, the percentage of electrons traveling close to and parallel to the axis is small. In addition, space-charge effects, radiofrequency instabilities, and random motions will tend to deflect electrons from the axis. Nevertheless, the axis of symmetry is the "weakest" spot and the only known deficiency of the electrostatic, axisymmetric collector and should be given proper attention.

Analytical Results

Figures 1 to 3 show electron trajectories for various beam parameters and collector configurations in the absence of magnetic focusing fields (i.e., $B = 0$). Figure 4(a) shows trajectories for magnetically focused beams which enter the collector after passing through a hole in an ideal magnetic shield ($B_{sat} = \infty$, $\mu = \infty$). All confined-flow focused beams experience a deflection during the transition from $B = B_t$ into $B = 0$, which is due to the flux at the cathode. This "magnetic" deflection is absent for Brillouin-focused ($\psi_c = 0$) and electrostatically focused beams. Although the rotational (magnetic) energy $(m/2)r^2(\sin^2 \vartheta)\dot{\varphi}^2$ at the apex is always small compared to the initial injection energy ϵ_i, $(m/2)r^2\dot{\vartheta}^2$ is large (e.g., $\geq 1/3\ \epsilon_i$) and the collector efficiency, particularly for the low-velocity classes, is relatively small for the equipotential configuration shown in figure 4(a). This deficiency can be much reduced, as shown in figure 4(b), by making the equipotentials more perpendicular to the trajectories at the apex.

It is important to shield the collector region (as perfectly as feasible) from the main focusing field for two reasons: First, the amount of rotational energy which cannot be recovered at impact is reduced. And second, "back focusing" of reflected primaries and generated secondaries into the interaction region of the tube along magnetic flux lines can be prevented.

In figures 1, 2, and 4 the space-charge density is small and affects the trajectories, compared to space-charge-free cases, only very little. In figure 3, computed for injection current densities of 30 and 90 amperes per square centimeter, the space-charge forces dominate the trajectories in the vicinity of the injection hole. Notice the heavy depression of equipotentials in the injection region. The spike has been removed en-

tirely in order not to obscure the space-charge effects. It may be seen that space charge provides too high a degree of sorting for low-energy classes because approximately one-half of the axial energy is transferred into radial energy, with a subsequent severe loss in collector efficiency. Notice further in figures 3(a) and (b) that the apex of the trajectory for energy class 0.2 is only slightly above the -0.1 equipotential line, yielding a collection efficiency for this class of approximately only 50 percent. In contrast to this case, the low-space-charge cases in figures 1, 2, and 4 show the energy at the apexes to approach 80 to 95 percent of their respective injection energy, thus permitting in principle a high collector efficiency. In addition, it is very difficult to make a planned velocity-sorting efficient in cases of space-charge-dominated flow. There is a danger of virtual cathode buildup and subsequent space-charge blocking and possible breakout of oscillations due to instabilities and fluctuations in high-space-charge densities. We must, therefore, conclude that a substantial dilution of high current densities down to a level of a few amperes per square centimeter or less at the injection hole is required if collector designs for higher-frequency tubes are to become feasible.

A possible arrangement to accomplish this task is shown in figure 5: the beam is permitted to expand in diameter by a factor of 5 or more, that is, the current density is decreased by a factor of 25 or more to the 1-ampere-per-square-centimeter level. A simple electrostatic lens compensates the outward radial electron velocity $+u_r$ by producing an inward component $-u_r$ on an electron located at radius r in the plane of the lens. Had all electrons exactly an outward radial velocity u_r which is strictly proportional to r, then an exact compensation of radial velocities would be possible and a close-to-parallel flow would enter the collector. Unfortunately, in a real spent electron stream, many electrons have radial velocities which are not strictly proportional to r and also the trajectories have positive and negative slopes near the lens due to a wide spread in velocities. Therefore, it will be possible, at best, to reduce, on the average, only a fraction of the radial spread, with a resulting substantial improvement in collector efficiency compared to entirely uncompensated cases. A magnetic lens permitting an oscillation-free adiabatic expansion to a larger Brillouin radius could be used for this purpose, as well as a combination of electric and magnetic fields. However, a more detailed discussion requires a precise knowledge of three-dimensional trajectories.

Relations Between Tube Efficiency, Collector Efficiency, and Overall Efficiency

A number of efficiency definitions are possible and needed by the tube designer and system engineer using the tube. Consider figure 6 on which the overall efficiency η_{ov} is plotted against the collector efficiency η_c with tube efficiency η_t as parameter. In

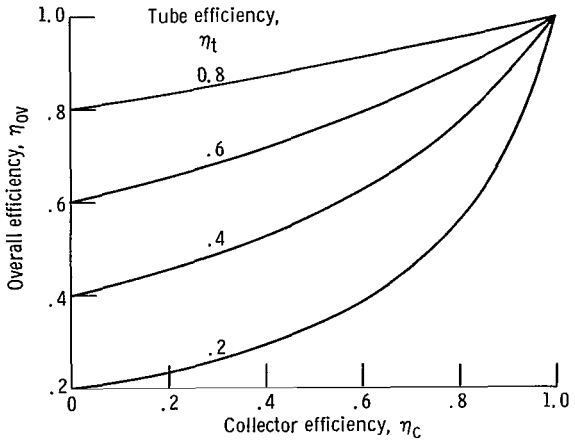

Figure 6. - Relation between overall tube efficiency and collector efficiency. $\eta_{ov} = \eta_t / [\eta_t \eta_c + (1 - \eta_c)]$.

this plot, circuit losses and interception losses prior to the collector are neglected. If P_o is the beam power $I_o V_o$, then

$$\eta_{ov} = \frac{\eta_t P_o}{P_o - (1 - \eta_t)\eta_c P_o} = \frac{\eta_t}{1 - \eta_c + \eta_c \eta_t} \tag{1}$$

$$\eta_t = \frac{P_{RF\text{-}out}}{P_o} \tag{2}$$

$$\eta_c = \frac{\sum_{k=1}^{n} I_k V_k}{(1 - \eta_t) P_o} \tag{3}$$

A more accurate formula is given in equation (4)

$$\eta_{ov} = \eta_{ct} \frac{\eta_e}{1 - \eta_c \left(1 - \eta_e - \frac{P_{int}}{P_o}\right)} \tag{4}$$

where η_{ct}, η_e, and P_{int} designate the circuit efficiency, electronic power conversion efficiency, and the power intercepted prior to entering the collector, respectively; P_{int} is difficult to determine but it can be written as $\langle \epsilon \rangle I_{int} / I_o$, where $\langle \epsilon \rangle$ is the

normalized average volt energy of the intercepted electrons and I_{int} is the intercepted current. At saturation $\langle \epsilon \rangle$ is usually between 0.1 and 0.8, depending on particular circumstances.

In equation (3) the summation is over n collector electrodes, each collecting a current I_k at a potential V_k below the potential zero of the output section of the tube. Thus, $\sum I_k \cdot V_k$ is the kinetic power in the spent beam recovered by the collector and $(1 - \eta_t)P_o$ is the kinetic beam power entering the collector. Note that η_t is less than the electronic efficiency of the tube η_e.

How does one optimize η_{ov}, the only efficiency of interest to the system designer? Although a quantitative answer is not yet available, a quantitative estimate can be easily produced. The electronic tube efficiency η_e is proportional to the square of the total beam coupling coefficient k^2 times the time average of the product $i_1(t)v_1(t) \cos \varphi(t)$, where $i_1(t)$ and $v_1(t)$ are the time-dependent amplitudes of the radiofrequency convection current and radiofrequency voltage, respectively, and $\varphi(t)$ is the phase between them. Thus,

$$\eta_e \sim k^2 \overline{i_1(t)v_1(t) \cos \varphi(t)}$$

The theoretical maximum of i_1 is $2 I_o$. In well-designed klystrons i_1 approaches values of 1.6 to 1.8 I_o, and in traveling wave tubes 1.2 to 1.4 I_o. The maximum of the radiofrequency output voltage v_1 must be smaller than that which causes the reflection of the slowest electron in the output gap (i.e., $v_1 \lesssim 1.1 V_o$). Although the adjustment of the output voltage to such a high value may produce an optimum of η_e, it certainly will not yield the highest possible η_{ov}. It is clear that the spent beam will contain many electrons with energies close to zero whose residual kinetic energy can not be recovered and which only cause high interception at undepressed potentials. In addition, such a stream will have a very high degree of axial and radial velocity spread, which makes effective sorting less efficient. We have to conclude, therefore, that an optimum η_{ov} in klystrons will probably occur at output radiofrequency voltages slightly less than those producing a maximum in η_e. A quantitative discussion would require the knowledge of exact three-dimensional trajectories.

In traveling wave tubes the situation is different. Because the TWT circuit impedance Z is smaller than in klystrons, the radiofrequency voltages v_1 are almost always well below V_o (e.g. $|v_1| \lesssim \frac{3}{4} V_o$), and the slowest electrons in the stream have still a significant kinetic energy. It appears, therefore, that depressed collectors should have a better potential of improving TWT efficiency than that of klystrons.

Collector Losses

It is appropriate at the conclusion of this discussion to review basic limitations and losses of this collector. Were exact velocity vectors known, it would then be possible to give an accurate account. In absence of such knowledge, only a useful estimate can be given.

An electrostatic collector requires a certain energy, fortunately only a small amount, to accomplish velocity-sorting. The amount of this energy which represents a basic loss of efficiency can be measured directly as the difference between the volt energy at the apex and the initial volt energy at the start. For small angular spread this difference can be made small, perhaps 5 to 10 percent.

Another source of losses stems from the finite number of collector plates. For a large number of plates the electrons will be losing roughly one-half of the potential difference between two adjacent stages. For a five-stage collector, this amounts to approximately 10 percent loss in efficiency, for a 20-stage collector only 2.5 percent loss. An additional loss results if there are electrons with energies larger than $-eV_{cath}$, where $V_{cath} < 0$ and no collector plates are below cathode potential. This loss is very significant in klystrons and less important in TWT's and may range between 5 and 25 percent. Still other losses may occur due to secondaries and ions, if present.

All the aforementioned deficiencies can be reduced to a tolerable minimum with careful design and effort. There is, however, still present a different source of deficiency which is much more difficult to control and eliminate than the aforementioned sources. This deficiency is related to inadequate velocity-sorting caused by large angular spreads and can be only partially eliminated with refocusing. In figure 1(b), for example, the electron of energy class 0.2 and starting with $6\frac{1}{2}^{o}$ will easily land on plate $V = -0.15\ V_o$. The same electron in figure 1(c) starting at 3^{o} will just miss the $-0.15\ V_o$ plate. Similar considerations apply to other trajectories. It is estimated that velocity-sorting losses can be reduced to 5 percent with refocusing.

It therefore appears feasible that a carefully designed collector with low space charge, a refocused beam, and having 10 or more stages may approach 80 to 90 percent recovery efficiency from a spent beam. This would represent a drastic improvement over older designs.

Figure 7 shows an artist's concept of the collector exposing the apertures and electron trajectories. Figure 8 shows the actual collector mounted on top of an S-band klystron amplifier. The individual electrodes are mounted in a rack and held separated by insulators.

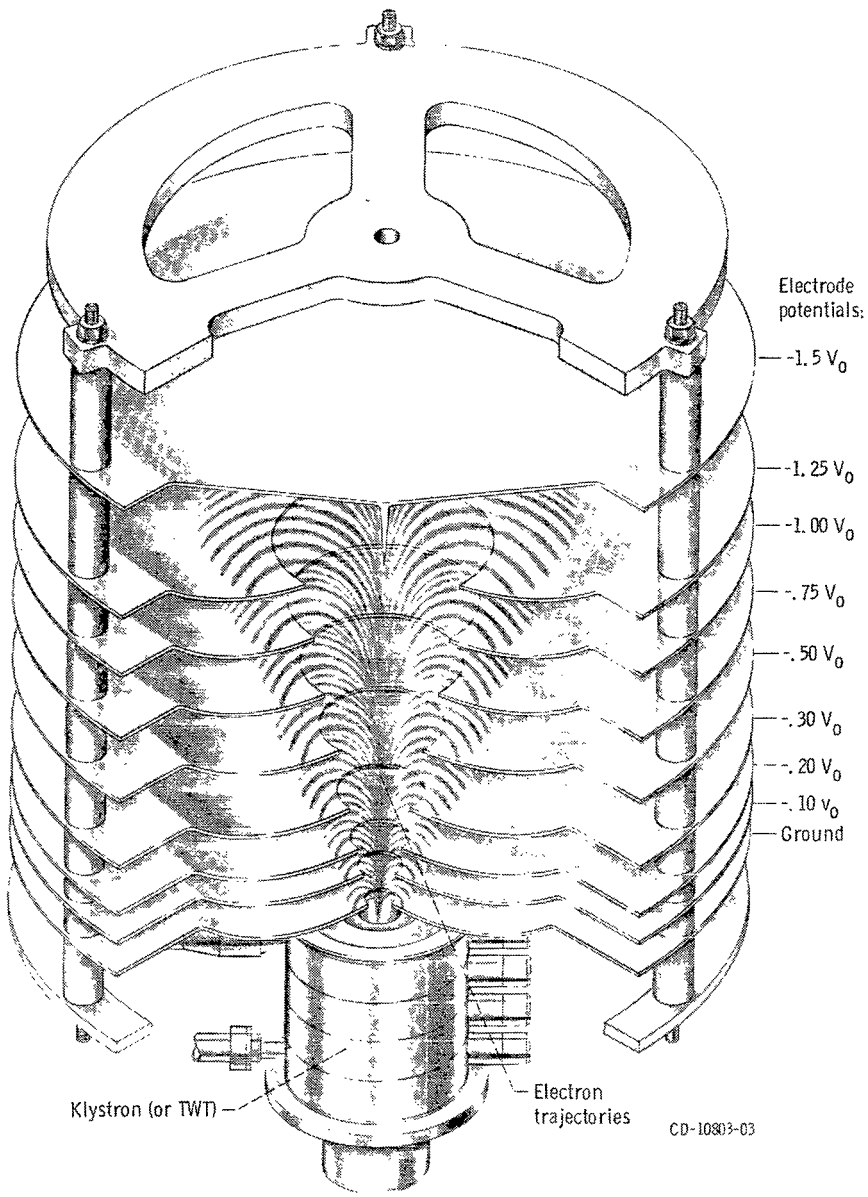

Figure 7. - Drawing of collector with exposed apertures and trajectories. ($V_0 = V_{cathode}$, with respect to ground.)

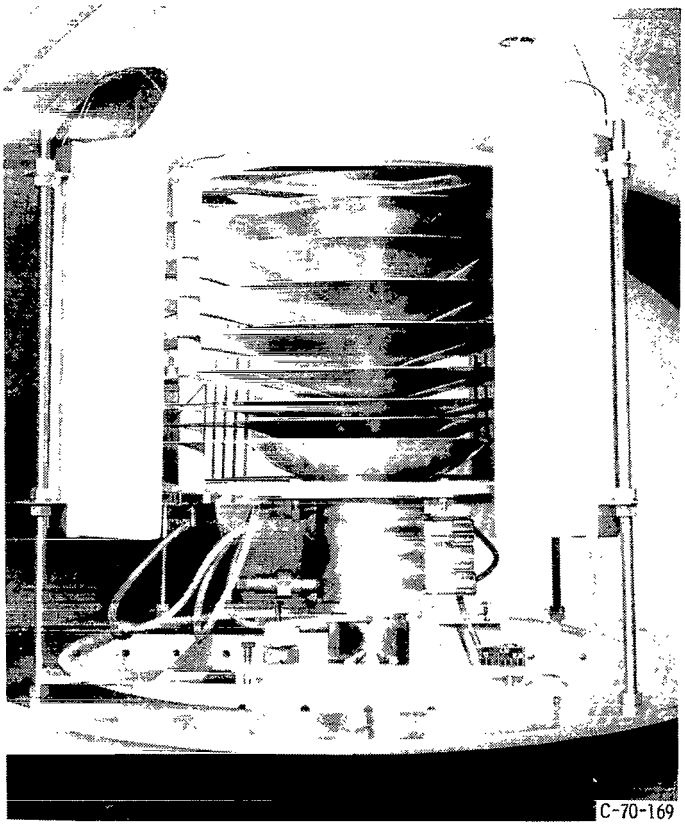

Figure 8. - Actual collector mounted on electron tube.

CONCLUSIONS

A model of an axisymmetric, electrostatic depressed collector for linear-beam-type microwave tubes is given. The model eliminates to a high degree the deficiencies of "older" depressed collectors and shows promise to work effectively even when applied to a spent beam with a large radial and axial velocity spread.

It is concluded that the geometry of the beam and the collector must be chosen such as to render space-charge effects relatively unimportant on trajectories and collector efficiency. In confined-flow focused beams, all electrons experience a deflection which results in a substantial loss in collector recovery efficiency for low-energy electrons and a small loss for higher energies. It is concluded that as small a ratio of the focusing field to the Brillouin field B/B_B as feasible should be used to enhance the collector efficiency. Such losses do not occur in focusing schemes where the magnetic field at the cathode is zero or small or when the beam has been refocused. A qualitative argument is derived for achieving an overall optimum efficiency for the tube-collector combination. A significant improvement in the state-of-art of tube-collector efficiency is believed to result with the optimization of the designs, with collector efficiencies approaching 90 percent for a less-than-10-electrode configuration.

Lewis Research Center,
National Aeronautics and Space Administration,
Cleveland, Ohio, September 16, 1970,
164-21.

APPENDIX A

SOLUTION OF THE BOUNDARY-VALUE PROBLEM WITH GREEN'S FUNCTION

Common electrical boundaries, such as a spark gap or a spike, can be well approximated by an axisymmetric conductor of the shape of a prolate ellipsoid of rotation. In the case of a spike approaching the shape of a sharp needle, the smaller semi-axis b of the prolate spheroid (e.g., an axisymmetric ellipsoid) may be shrunk to the limit zero or to any other fraction $b/c < 1$, where c is the larger semi-axis.

We solve the boundary-value problem with the method of Green's function. After the Green's function appropriate to the selected geometry has been found, the determination of the potential is reduced to a quadrature by means of the equation

$$V(P) = \int_{\text{volume}} G(P, P_o) \cdot \rho_\epsilon(P_o)\, d\mathscr{V}_o + \epsilon_o \int_{\text{surface}} V_S(S) \left(\frac{\partial G}{\partial \bar{n}}\right)_S dS \tag{A1}$$

Here $G(P, P_o)$ is the Green's function of reference points P and source points P_o, ρ_e is the space-charge density inside the volume $\mathscr{V}_o$ bounded by the surface S along which the potential is V_S.

To derive the Green's function for our basic configuration of a cone with an included half-angle ϑ, a spike at its apex represented by the two semi-axes c and b and surrounded by a sphere of radius R (see fig. 9), we use the coordinate system η, ξ, and φ of spheroids of rotation. The coordinates η and ξ are related with the coordinates z and r in the cylindrical coordinate system by the equations (ref. 6, ch. 5.28):

$$z = c_2 \eta \xi \tag{A2}$$

$$r = c_2 \left[(1 - \xi^2)(\eta^2 - 1)\right]^{1/2} \tag{A3}$$

where

$$c_2 = (c^2 - b^2)^{1/2} = \text{Linear eccentricity} \tag{A4}$$

The third coordinate is, of course, the polar angle φ. Now, the equation of a cone is

$$\cos \vartheta = \frac{z}{(z^2 + r^2)^{1/2}} = \text{Constant} \tag{A5}$$

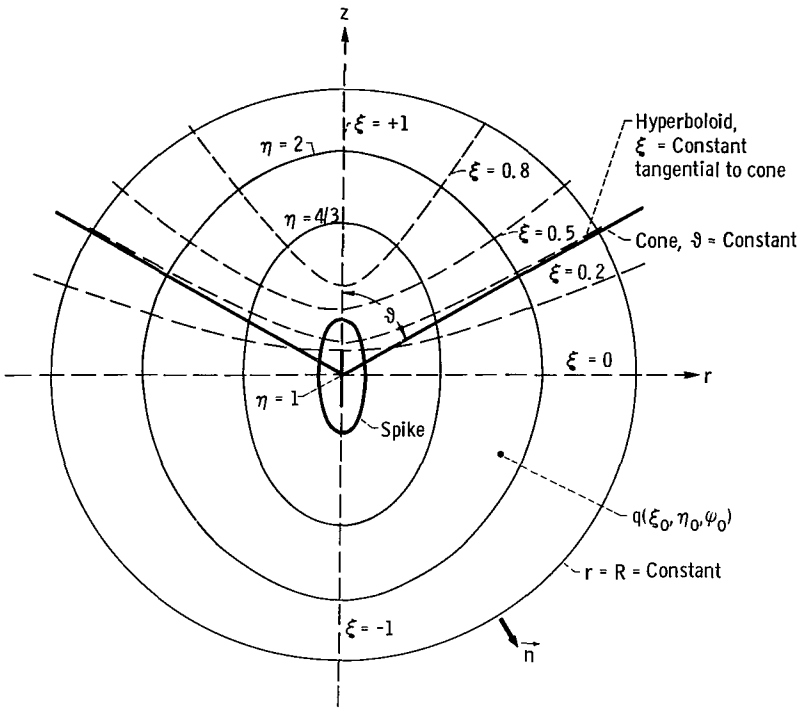

Figure 9. - Derivation of Green's function in spheroidal (elliptical) harmonics.

Substituting equations (A3) and (A4) into equation (A5) yields

$$\left.\begin{aligned} \cos\vartheta &= \frac{\eta\xi}{\sqrt{\eta^2 + \xi^2 - 1}} \\ \text{or} \qquad \xi &= \cos\vartheta\left(\frac{\eta^2 - 1}{\eta^2 - \cos^2\vartheta}\right)^{1/2} \end{aligned}\right\} \tag{A6}$$

Putting $\cos\vartheta = \text{Constant} = \mu_c$ into equation (A5) we obtain on the surface of the cone

$$\xi_c = \mu_c\left(\frac{\eta^2 - 1}{\eta^2 - \mu_c^2}\right)^{1/2} = \mu_c\left[\frac{\eta^2 - 1}{(\eta^2 - 1) + (1 - \mu_c^2)}\right]^{1/2} = \mu_c\left(\frac{1}{1 + \dfrac{1 - \mu_c^2}{\eta^2 - 1}}\right)^{1/2}$$

$$\approx \mu_c\left(1 - \frac{1}{2}\frac{1 - \mu_c^2}{\eta^2 - 1} + \frac{3}{8}\frac{(1 - \mu_c^2)^2}{(\eta^2 - 1)^2} - + \cdots\right)$$

The difference between ξ_c and μ_c is largest for $\xi_c = 1$ and diminishes to zero as η becomes large. Thus deviations between ξ_c and μ_c occur only at the joint of the spike and the cone, where no trajectories are present. A hyperboloid

$$-\frac{z^2}{c_2^2\xi_c^2} + \frac{r^2}{c_2^2(1 - \xi_c^2)} = 1$$

could be used exactly in place of the cone to preset the inclination of the equipotentials (see fig. 9), the only reservation being that a curved surface is more difficult to produce than a cone. To obtain the expression for the Green's function, write the general solution of Laplace's equation in coordinates of a prolate spheroid:

$$V = \sum_n \sum_m \Xi_{mn} H_{mn} \Phi_m \tag{A7}$$

with

$$\Xi_{mn} = AP_n^m(\xi) + BQ_n^m(\xi) \tag{A8a}$$

$$H_{mn} = A'P_n^m(\eta) + B'Q_n^m(\eta) \tag{A8b}$$

$$\Phi_m = c \cos m\varphi + D \sin m\varphi \tag{A8c}$$

Since we seek a solution which is finite everywhere, including the origin and infinity, we must reject $Q_n^m(\xi)$ inside because $\lim_{\xi \to 1} Q(\xi) = \infty$, and $P(\eta)$ outside since $\lim_{\eta \to \infty} P(\eta) = \infty$. The range of the independent variables η and ξ appearing in the formulation of equation (7) is $1 < \eta < \infty$; $-1 \leq \xi \leq +1$. Because in the presence of the spike the line $\eta = 1$ is excluded, $Q(\eta)$ must be admitted. Since our problem involves conical boundaries, the

solution (eqs. (7) and (8)) must be expanded in terms of harmonics with noninteger values n so chosen that the $P_n^m(\xi)$ are zero on the cones. That is, $P_n^m(\xi_c) = 0$, thus satisfying the equipotential requirement on the surface of the cone, $\cos \vartheta = \mu_c \approx \xi_c =$ Constant. Since for noninteger values n $P_n(\xi)$ has a logarithmic singularity at $\xi = +1$, we must use the function $P_n(-\xi)$, which is regular in the region $\vartheta > 0$, where Green's function is derived.

To solve this problem, proceed as follows: The potential of a point charge q located at η_o, ξ_o, and φ_o facing an earthed cone (μ_c = Constant) alone (i.e., at first, without a spike and sphere) would be

$$V_{ic} = \sum_n \sum_{m=0}^{\infty} A_{mn} P_n^m(-\xi) P_n^m(\eta) Q_n^m(\eta_o) \cos m(\varphi - \varphi_o) \tag{A9}$$

for $\eta \leq \eta_o$, and

$$V_{oc} = \sum_n \sum_{m=0}^{\infty} A_{mn} P_n^m(-\xi) Q_n^m(\eta) P_n^m(\eta_o) \cos m(\varphi - \varphi_o) \tag{A10}$$

for $\eta \geq \eta_o$. It may be verified, by inspection of equations (A9) and (A10), that $V_{ic} = V_{oc}$ at $\eta = \eta_o$, and that both solutions are finite everywhere and symmetric about the charge point ξ_o, η_o, φ_o. Also, $V_{ic} = V_{oc} = 0$ on the cone because of our choice of $P_n^m(\xi_c) = 0$.

Suppose now that the charge q is placed between an earthed sphere of radius R and the cone with an ellipsoidal spike attached at the cone's apex (fig. (9)). The contour of the spike is given by $\eta = \eta_S$ = Constant. We must now superimpose on the potential of the cone another potential that will be zero on the cone and will give a resultant zero potential when $\eta = \eta_S$ on the spike and $\eta = \eta_R$ on the sphere R. For the spheroid with the semi-axes c and b,

$$\eta_S = \frac{c}{\sqrt{c^2 - b^2}} = \frac{c}{c_2} \tag{A11}$$

and, from equations (A2) and (A3),

$$\eta_R^2 = \frac{R^2}{c^2 - b^2} + 1 - \xi^2 \approx \frac{R^2}{c^2 - b^2} + 1 \tag{A12}$$

to a high degree independent of ξ, because $\xi < 1$ and $R/c >> 1$. Notice that, since a

spheroidal coordinate system is used, the spheroidal surface $\eta = \eta_S$ can be expressed by a single value η_S for the entire range of the other coordinates, ξ and φ. But two coordinates, η and ξ are needed (eq. (A12)) to describe exactly a spherical surface (R = Constant). Since now in figure 6, both $\eta = 1$ and $\eta = \infty$ are excluded, the superimposed potential V_{si} must have the linear combination $B_{mn}P_n^m(\eta) + C_{mn}Q_n^m(\eta)$. Thus,

$$V_{si} = \sum_n \sum_m^{\infty} A_{mn}P_n^m(-\xi)\left[B_{mn}P_n^m(\eta) + C_{mn}Q_n^m(\eta)\right]\cos m(\varphi - \varphi_o) \tag{A13}$$

When equation (A13) is added to equation (A9) taken at $\eta = \eta_S$, the result is zero:

$$(V_{ic} + V_{si})_{\eta=\eta_S} = 0 = P_n^m(\eta_S)Q_n^m(\eta_o) + B_{mn}P_n^m(\eta_S) + C_{mn}Q_n^m(\eta_S) \tag{A14}$$

And when $\eta = \eta_R$ on the sphere, $V_{oc} + V_{si}$ is zero:

$$(V_{oc} + V_{si})_{\eta=\eta_R} = 0 = Q_n^m(\eta_R)P_n^m(\eta_o) + B_{mn}P_n^m(\eta_R) + C_{mn}Q_n^m(\eta_R) \tag{A15}$$

When equations (A14) and (A15) are solved for B_{mn} and C_{mn},

$$B_{mn} = Q_n^m(\eta_R)\frac{P_n^m(\eta_o)Q_n^m(\eta_S) - P_n^m(\eta_S)Q_n^m(\eta_o)}{P_n^m(\eta_S)Q_n^m(\eta_R) - P_n^m(\eta_R)Q_n^m(\eta_S)} \tag{A16}$$

$$C_{mn} = -P_n^m(\eta_S)\frac{P_n^m(\eta_o)Q_n^m(\eta_R) - P_n^m(\eta_R)Q_n^m(\eta_o)}{P_n^m(\eta_S)Q_n^m(\eta_R) - P_n^m(\eta_R)Q_n^m(\eta_S)} \tag{A17}$$

Adding this new potential V_{si} to V_{ic} yields the complete potential V_i, when $\eta_S < \eta < \eta_o$

$$V_i = \sum_n \sum_{m=0}^{\infty} A_{mn}P_n^m(-\xi)\left\{\left[B_{mn} + Q_n^m(\eta_o)\right]P_n^m(\eta) + C_{mn}Q_n^m(\eta)\right\}\cos m(\varphi - \varphi_o) \tag{A18}$$

And similarly, when $\eta_o < \eta < \eta_R$

$$V_o = \sum_n \sum_{m=0}^{\infty} A_{mn} P_n^m(-\xi) \left\{ B_{mn} P_n^m(\eta) + \left[P_n^m(\eta_o) + C_{mn} \right] Q_n^m(\eta) \right\} \cos m(\varphi - \varphi_o) \qquad \text{(A19)}$$

To determine the constant A_{mn}, a new variable $\varphi' = \varphi - \varphi_o$ is introduced and an expression for the flux density originating in the surface $\eta = \eta_o$ of the charge is written. This expression is evaluated by invoking Gauss' theorem applied to a box fitting closely an element of the spheroid η_o. Using $\bar{n}$ for a "normal" (while n denotes the harmonic number),

$$\sigma_{\bar{n}} = \epsilon_o \left(\frac{\partial V_i}{\partial \bar{n}} - \frac{\partial V_o}{\partial \bar{n}} \right)_{\eta=\eta_o} = \frac{\epsilon_o}{h_2} \left(\frac{\partial V_i}{\partial \eta} - \frac{\partial V_o}{\partial \eta} \right)_{\eta=\eta_o} \qquad \text{(A20)}$$

Here, h_1, h_2, and h_3 are the metric coefficients (distance factors) appropriate to the orthogonal curvilinear coordinates of our spheroids. Specifically,

$$h_1 = c_2 \left(\frac{\eta^2 - \xi^2}{1 - \xi^2} \right)^{1/2} \qquad \text{(A21a)}$$

$$h_2 = c_2 \left(\frac{\eta^2 - \xi^2}{\eta^2 - 1} \right)^{1/2} \qquad \text{(A21b)}$$

$$h_3 = r = c_2 \sqrt{(1 - \xi^2)(\eta^2 - 1)} \qquad \text{(A21c)}$$

Returning now to equation (A20), the indicated differentiation may be completed with the help of equations (A21b), (A18), and (A19):

$$\sigma_{\bar{n}} = \frac{\epsilon_o}{c_2} \left(\frac{\eta^2 - 1}{\eta^2 - \xi^2} \right)^{1/2} \sum_n \sum_{m=0}^{\infty} A_{mn} P_n^m(-\xi) \cos m\varphi' \left[Q_n^m(\eta_o) P_n'^m(\eta) - Q_n'^m(\eta) P_n^m(\eta_o) \right]_{\eta=\eta_o} \qquad \text{(A22)}$$

where the prime on P and Q indicates differentiation $\partial / \partial \eta$. Since our charge q at ξ_o, η_o, and φ_o is a point charge, the function $P_s^p(-\xi)_{\xi=\xi_o}$ assumes in the limit the constant value $P_s^p(-\xi_o)$.

Multiplying the left side of equation (A22) by $P_s^p(-\xi)\cos p\varphi' \cdot h_1 \cdot h_3 \times d\xi\, d\varphi'$ and integrating over the surface of the spheroid within the cone at $\eta = \eta_o$ gives

$$\int_{\varphi'=0}^{2\pi}\int_{\xi=-1}^{\xi_c} \dot{\sigma}_{\overline{n}} \cdot P_s^p(-\xi)\cos p\varphi' h_i h_3\, d\xi\, d\varphi' = \int_0^{2\pi}\int_{-1}^{\xi_c} \sigma_{\overline{n}} P_n^p(-\xi)\cos p\varphi' \cdot \overrightarrow{dS} \qquad \text{(A23)}$$

Now

$$\sigma_{\overline{n}} = \left(\frac{\partial V_i}{\partial \overline{n}} - \frac{\partial V_o}{\partial \overline{n}}\right)\epsilon_o \Bigg|_{\eta=\eta_o}$$

is continuous across the spheroid except over the infinitesimal area $\overrightarrow{dS}_o$ at $\varphi = \varphi_o$ or $\varphi' = 0$ ($\cos p\varphi' = 1$), where the charge is located. Thus $\partial V_i/\partial \overline{n} = \partial V_o/\partial \overline{n}$ except over $\overrightarrow{dS}_o$, and the integral vanishes elsewhere. Therefore, by Gauss' flux theorem

$$\int_0^{2\pi}\int_{-1}^{\xi_c} P_s^p(-\xi)\cos p\varphi' \cdot \sigma_{\overline{n}} \cdot \overrightarrow{dS} = q \cdot P_s^p(-\xi_o) \qquad \text{(A24)}$$

Now multiplying the right side of equation (A22) by the same factor as before yields

$$\frac{\epsilon_o}{c_2}\int_0^{2\pi}\int_{-1}^{\xi_c}\sum_n\sum_{m=0}^{\infty} A_{mn}\cos m\varphi' \cos p\varphi' P_n^m(\xi)P_s^p(\xi)\left[Q_n^m(\eta_o)P_n'^m(\eta) - Q_n'^m(\eta)P_n^m(\eta_o)\right]_{\eta=\eta_o}$$

$$\times\left(\frac{\eta^2-1}{\eta^2-\xi^2}\right)^{1/2} c_2^2\left(\frac{\eta^2-\xi^2}{1-\xi^2}\right)^{1/2}(1-\xi^2)(\eta^2-1)^{1/2}\Bigg|_{\eta=\eta_o} d\varphi'\, d\xi$$

$$= \sum_n\sum_{m=0}^{\infty} \epsilon_o c_2(\eta_o^2-1)(2-\delta_o^m)\pi A_{mn}\left[Q_n^m(\eta_o)P_n'^m(\eta_o) - Q_n'^m(\eta_o)P_n^m(\eta_o)\right]\times\int_{-1}^{\xi_c}\left[P_n^m(\xi)\right]^2 d\xi \qquad \text{(A25)}$$

because the integral over $d\varphi'$ is zero unless $p \equiv m$ and the integral over $d\xi$ is also zero for $s \neq n$. But a fundamental relation of spherical harmonics gives (ref. 6, ch. 5.212)

$$Q_n^m(\eta_o)P_n'^m(\eta_o) - Q_n'^m(\eta_o)P_n^m(\eta_o) = \frac{(-1)^m\,(n+m)!}{(\eta_o^2 - 1)(n-m)!} \tag{A26}$$

where for noninteger values of n

$$\left.\begin{aligned}(n+m)! &= \int_0^\infty t^{(n+m)}\, e^{-t}\, dt \\ (n-m)! &= \int_0^\infty t^{(n-m)}\, e^{-t}\, dt\end{aligned}\right\} \tag{A27}$$

and

$$\int_{-1}^{\xi_c} \left[P_n^m(-\xi)\right]^2 d\xi = \frac{1-\xi_c^2}{2n+1}\left[\frac{\partial P_n^m(-\xi)}{\partial \xi}\,\frac{\partial P_n^m(-\xi)}{\partial n}\right]_{\xi=\xi_c} \tag{A28}$$

Thus, from equations (A24) to (A26), and (A28)

$$A_{mn} = \frac{\dfrac{(2-\delta_m^o)(-1)^m}{2\pi\epsilon_o c_2(1-\xi_c^2)}\, q \cdot P_n^m(-\xi_o)\dfrac{(n-m)!}{(n+m)!}\,(2n+1)}{\left(\dfrac{\partial P_n^m(-\xi)}{\partial \xi}\,\dfrac{\partial P_n^m(-\xi)}{\partial n}\right)_{\xi=\xi_c}} \tag{A29}$$

We are now prepared to write the expression for Green's function $G(P, P_o)$, P and P_o having the coordinates ξ, η, φ and ξ_o, η_o, φ_o of the reference point and source point, respectively. Putting q = 1 (unit charge) into equation (A29), we get from equations (A18) and (A19)

$$G_i(P, P_o) = \sum_n \sum_{m=0}^{\infty} A_{mn} P_n^m(-\xi)\left\{\left[B_{mn} + Q_n^m(\eta_o)\right]P_n^m(\eta) + C_{mn}Q_n^m(\eta)\right\}\cos m(\varphi - \varphi_o) \tag{A30}$$

for $\eta_S \le \eta \le \eta_o$, and

$$G_o(P, P_o) = \sum_{n}\sum_{m=0}^{\infty} A_{mn} P_n^m(-\xi)\left\{B_{mn} P_n^m(\eta) + \left[C_{mn} + P_n^m(\eta_o)\right] Q_n^m(\eta)\right\} \cos m(\varphi - \varphi_o) \quad \text{(A31)}$$

for $\eta_o < \eta \leq \eta_R$

For a given space-charge density distribution $\rho_e(P_o)$ inside the sphere R and a given potential distribution $V = V_S$ on the surface of the sphere, the exact expression for the potential V(P) at any point P located inside the space bounded by the sphere, cones, and spike is given by equation (A1):

$$V(P) = \int_{\text{volume}} G(P, P_o) \cdot \rho_e(P_o)\, d\mathscr{V}_o + \epsilon_o \int_{\text{surface}} V_S(P_S) \left(\frac{\partial G_o}{\partial \vec{n}}\right)_{\eta=\eta_R} \vec{dS} \quad \text{(A1)}$$

In the volume integral the integration needs to be extended only over regions where $\rho_e \neq 0$, that is, where trajectories exist. The second integral requires the knowledge of the normal derivative of G_o at the spherical surface. In analogy to equation (A20),

$$\left.\begin{aligned} \left(\frac{\partial G_o}{\partial \vec{n}}\right)_{\eta=\eta_R} &= \frac{1}{h_2}\left(\frac{\partial G_o}{\partial \eta}\right)_{\eta=\eta_R} = \frac{1}{c_2}\left(\frac{\eta_R^2 - 1}{\eta_R^2 - \xi^2}\right)^{1/2} \\ &\times \sum_{n}\sum_{m=0}^{\infty} A_{mn} P_n^m(-\xi)\left\{B_{mn} P_n'^m(\eta_R) + \left[P_n^m(\eta_o) + C_{mn}\right] Q_n'^m(\eta_R)\right\} \cos m(\varphi - \varphi_o) \\ P' &= \left.\frac{\partial P}{\partial \eta}\right|_{\eta=\eta_R} \\ Q' &= \left.\frac{\partial Q}{\partial \eta}\right|_{\eta=\eta_R} \end{aligned}\right\} \quad \text{(A32)}$$

Substituting equation (A29) for A_{mn}, and equations (A16) and (A17) for B_{mn} and C_{mn}, respectively, and carrying out the indicated differentiations in equation (A32) yields

$$\left(\frac{\partial G_o}{\partial \bar{n}}\right)_{\eta=\eta_R} = \frac{(2 - \delta_m^o)(2n + 1)}{2\pi\epsilon_o(c^2 - b^2)(1 - \xi_c^2)(\eta_R^2 - \xi^2)^{1/2}(\eta_R^2 - 1)^{1/2}}$$

$$\times \sum_n \sum_{m=0}^{\infty} P_n^m(-\xi_o) \frac{Q_n^m(\eta_S)P_n^m(\eta_o) - P_n^m(\eta_S)Q_n^m(\eta_o)}{P_n^m(\eta_S)Q_n^m(\eta_R) - P_n^m(\eta_R)Q_n^m(\eta_S)} \cos m(\varphi - \varphi_o)$$

$$\times \frac{1}{\left(\frac{\partial P_n^m(-\xi)}{\partial \xi} \frac{\partial P_n^m(-\xi)}{\partial n}\right)_{\xi=\xi_c}} \tag{A33}$$

Sometimes it is advantageous not to have the spike, if, for example, the potential depression and velocity-sorting due to a large space charge itself are stronger than desired. In this case, there is no need to use expansions in elliptical harmonics, but rather spherical functions are appropriate. We still use noninteger orders n of $P_n^m(-\mu)$ such that, on the cone, $P_n^m(-\mu_c) = 0$. We forego the now much simpler derivation of the Green's function for a cone ϑ_c surrounded by a sphere of radius R and write the expressions for G_i^o, G_o^o, and $(\partial G_o^o/\partial r)_{r=R}$ (the superscript o denoting the absence of the spike).

$$G_i^o = \sum_n \sum_{m=0}^{\infty} A_{mn} P_n^m(-\mu) \cdot \left(\frac{r}{r_o}\right)^n \left[1 - \left(\frac{r_o}{R}\right)^{(2n+1)}\right] \cos m(\varphi - \varphi_o) \tag{A34}$$

$$G_o^o = \sum_n \sum_{m=0}^{\infty} A_{mn} P_n^m(-\mu)\, r_o^{(n+1)} \left(\frac{1}{r^{n+1}} - \frac{r^n}{R^{(2n+1)}}\right) \cos m(\varphi - \varphi_o) \tag{A35}$$

$$\left(\frac{\partial G_o^o}{\partial \bar{n}}\right)_{r=R} = \left(\frac{\partial G_o^o}{\partial r}\right)_{r=R} = -(2n+1)\frac{r_o^{n+1}}{R^{n+2}} \sum_n \sum_{m=0}^{\infty} A_{mn} P_n^m(-\mu) \cos m(\varphi - \varphi_o) \tag{A36}$$

$$A_{mn} = \frac{2 - \delta_m^o}{2\pi \epsilon_o \mu_o (1 - \mu_c^2)} \frac{P_n^m(-\mu_o)}{\left[\frac{\partial P_n^m(-\mu)}{\partial \mu} \frac{\partial P_n^m(-\mu)}{\partial n}\right]_{\mu=\mu_c}} \tag{A37}$$

APPENDIX B

TRAJECTORY EQUATIONS FROM LAGRANGIAN FORMULATION

The basic geometrical configuration of the tube-collector arrangement is shown in figure 10. After leaving the last interaction gap, the spent electron stream passes through the fringes of the focusing magnetic field, if any, which leaks through the 2a opening in an ideal (magnetic) shield into the collector region. Although sperical (or spheroidal) coordinates are most suitable for the trajectories inside, cylindrical coordinates lend themselves best for the transition region, which consists of a cylindrical tube terminated by the shielding plane which merges into the collector region. We

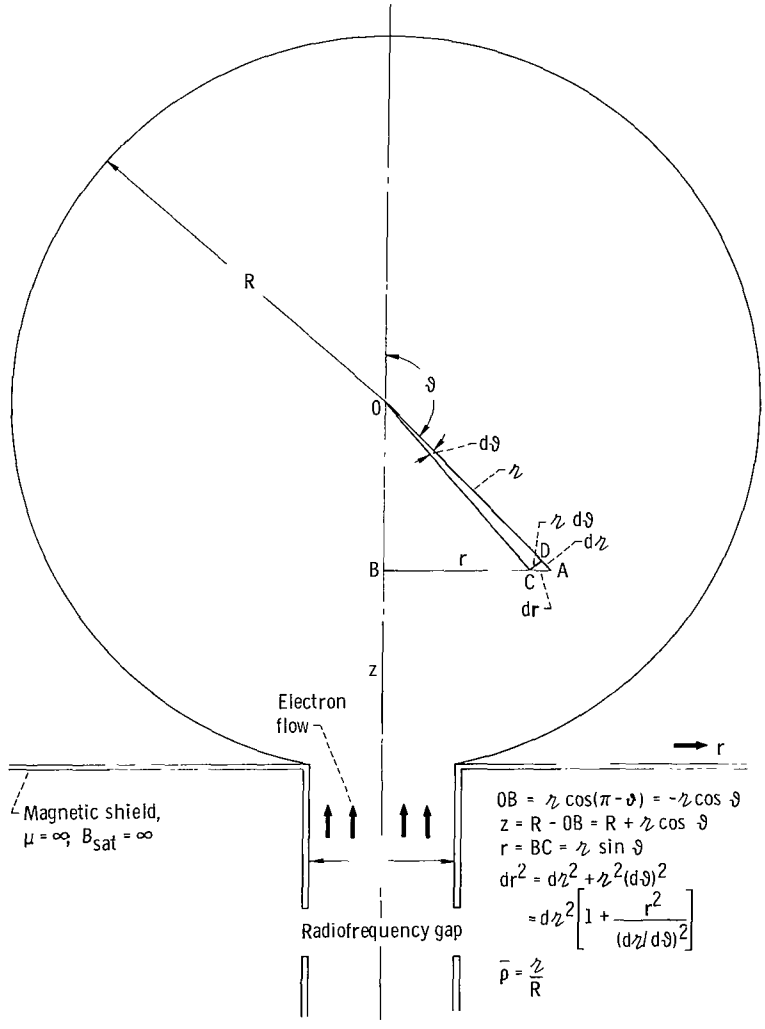

Figure 10. -Transition through magnetic shield.

shall develop first the trajectory equations in spherical coordinates r, ϑ, and φ; ϑ and φ being the polar angle and the azimuth, respectively. The magnetic field is axisymmetric and derivable from the only components $A_\varphi(r, z)$ of the vector potential A, or a corresponding scalar potential V_m. The expression for the generalized Lagrangian L^* of a particle with a charge q is

$$L^* = T - q \cdot V + q\vec{u} \cdot \vec{A}$$

and for an electron with a charge $q = -e$

$$L^* = T + eV - e\vec{u} \cdot \vec{A}$$

Hereinafter e shall indicate the amount of the electronic charge $e = +1.6\times10^{-19}$ coulombs, the sign having been taken care of. In our case of spherical coordinates,

$$L^* = \frac{1}{2} m\left[\dot{r}^2 + r^2\dot{\vartheta}^2 + r^2(\sin^2\vartheta)\,\dot{\varphi}^2\right] + eV - er\dot{\varphi}(\sin\vartheta)A_\varphi(r, \vartheta) \tag{B1}$$

In equation (B1), $A_\varphi(r, \vartheta)$ is assumed to have been transformed from $A_\varphi(r, z)$ by means of the relations shown in figure 10:

$$r = r \sin\vartheta \tag{B2}$$

$$z = R - OB = R + r\cos\vartheta \tag{B3}$$

$$dr^2 = dr^2 + r^2(d\vartheta)^2 = dr^2\left[1 + \frac{r^2}{\left(\frac{dr}{d\vartheta}\right)^2}\right] \tag{B4}$$

Here, r, φ, z are the cylindrical coordinates, and r, ϑ, φ the spherical coordinates. The momentum equations are obtained from

$$\frac{d}{dt}(\nabla_{\dot{q}} L^*) - \nabla_q L^* = 0 \tag{B5}$$

where q and $\dot{q}$ are the coordinates and the rate of change of coordinates with time, respectively. To evaluate equation (B5) we need to know the expression $\dot{A} = dA/dt$, which appears in some components of equation (B5). Since $A \equiv A_\varphi(r, \vartheta)$ has only one component A_φ and $\partial A_\varphi / \partial\varphi = 0$,

$$\dot{A}_\varphi = \frac{dA_\varphi}{dt} = \frac{\partial A_\varphi}{\partial t} + \sum_k \frac{\partial A_\varphi}{\partial q_k}\dot{q}_k = \dot{\blacksquare}\frac{\partial A_\varphi}{\partial \blacksquare} + \dot{\vartheta}\frac{\partial A_\varphi}{\partial \vartheta} \tag{B6}$$

The application of the Lagrangian routine to equation (B1) yields the following components for the equations of motion:

$$\left.\begin{aligned} &\ddot{\blacksquare} - \blacksquare(\sin^2\vartheta)\dot{\varphi}^2 - \blacksquare\dot{\vartheta}^2 - \eta_e\left[\frac{\partial V}{\partial \blacksquare} - A_\varphi(\sin\vartheta)\dot{\varphi} - \blacksquare(\sin\vartheta)\dot{\varphi}\frac{\partial A_\varphi}{\partial \blacksquare}\right] = 0 \\ \text{or} \\ &\ddot{\blacksquare} - \blacksquare(\sin^2\vartheta)\dot{\varphi}^2 - \blacksquare\dot{\vartheta}^2 - \eta_e\left\{\frac{\partial V}{\partial \blacksquare} - \blacksquare(\sin\vartheta)\dot{\varphi}\left[-B_\vartheta(\blacksquare, \vartheta)\right]\right\} = 0 \end{aligned}\right\} \tag{B7a}$$

$$2\blacksquare\dot{\blacksquare}\dot{\vartheta} + \blacksquare^2\ddot{\vartheta} - \blacksquare^2\sin\vartheta(\cos\vartheta)\dot{\varphi}^2 - \eta_e\left[\frac{\partial V}{\partial \vartheta} - \blacksquare(\cos\vartheta)\dot{\varphi}A_\varphi - r(\sin\vartheta)\dot{\varphi}\frac{\partial A_\varphi}{\partial \vartheta}\right] =$$

$$= 2\blacksquare\dot{\blacksquare}\dot{\vartheta} + \blacksquare^2\ddot{\vartheta} - \blacksquare^2\sin\vartheta(\cos\vartheta)\dot{\varphi}^2 - \eta_e\left[\frac{\partial V}{\partial \vartheta} + \eta_e\blacksquare^2(\sin\vartheta)\dot{\varphi}\cdot B_\blacksquare(\blacksquare, \vartheta)\right] = 0 \tag{B7b}$$

$$2\left[\blacksquare(\sin\vartheta)\dot{\varphi} + \blacksquare(\cos\vartheta)\dot{\varphi}\dot{\vartheta}\right] + \blacksquare(\sin\vartheta)\ddot{\varphi} + \eta_e A_\varphi\left[\frac{\dot{\blacksquare}}{\blacksquare} + (\cos\vartheta)\dot{\vartheta} + \frac{\dot{A}_\varphi}{A_\varphi}\right] = 0 \tag{B7c}$$

In place of equation (B7c), we shall use Busch's theorem for determining $\dot{\varphi}$. From Busch's theorem for axisymmetric magnetic fields,

$$\dot{\varphi} = \frac{\eta_e}{2\pi r^2}\left[\psi(r,z) - \psi_o(r_o, z_o)\right] \equiv \dot{\varphi}(\blacksquare, \vartheta) \tag{B8}$$

$$\psi(r,z) = 2\pi\int_0^{\bar{r}=r} B_z(\bar{r}, z)\bar{r}\,d\bar{r} \equiv \psi(\blacksquare, \vartheta) \tag{B9}$$

and $\psi_o(r_o, z_o)$ represents the initial magnetic flux of the electron at r_o, z_o at the time of its start from the cathode surface. In equation (B8) cylindrical coordinates were used for $\dot{\varphi}$ and the fluxes ψ in agreement with our previous scheme. The expressions for

A_φ and $B = \text{curl } A = -\text{grad } V_m$ in both coordinate systems are given in appendix D, together with the exact solution for an axisymmetric magnetic field bounded by an ideal shield with an opening hole.

The use of equation (B8) permits the elimination of $\dot{\varphi}$ from equations (B7). To eliminate the time dependence, the expression for the velocity $u(\spadesuit, \vartheta, \varphi)$ is used in the collector region, assuming, as before, steady-state case:

$$u^2 = \left(\frac{d\spadesuit}{dt}\right)^2 + \spadesuit^2 \left(\frac{d\vartheta}{dt}\right)^2 + \spadesuit^2 \sin^2 \vartheta \left(\frac{d\vartheta}{dt}\right)^2 \tag{B10}$$

and

$$\frac{d\spadesuit}{dt} = \frac{\partial \spadesuit}{\partial \vartheta}\dot{\vartheta} + \frac{\partial \spadesuit}{\partial \varphi}\dot{\varphi} = \frac{\partial \spadesuit}{\partial \vartheta}\dot{\vartheta} = \spadesuit'\dot{\vartheta} \tag{B11}$$

because $\partial\spadesuit/\partial\varphi = 0$. Substitution of equation (B11) into equation (B10) yields

$$u^2(\spadesuit, \vartheta, \varphi) = (\spadesuit'\dot{\vartheta})^2 + (\spadesuit\dot{\vartheta})^2 + (\spadesuit \sin \vartheta\, \dot{\varphi})^2 = \spadesuit^2\dot{\vartheta}^2\left[1 + \left(\frac{\spadesuit'}{\spadesuit}\right)^2\right] + \spadesuit^2 \sin^2 \vartheta\, \dot{\varphi}^2$$

$$= \spadesuit^2\dot{\vartheta}^2\left[1 + \left(\frac{\spadesuit'}{\spadesuit}\right)^2\right] + \frac{\eta_e^2}{4\pi^2}\,\frac{1}{\spadesuit^2 \sin^2 \vartheta}\left[\psi(\spadesuit, \vartheta) - \psi_o\right]^2 \tag{B12}$$

Now, for an electron entering the opening hole at a position $r = R$ and $\vartheta = \vartheta_i$ with a velocity $u_i(\vartheta_i)$, its velocity $u^2(\spadesuit, \vartheta, \varphi)$ will be (writing $\spadesuit = \bar{\rho}R$, $\bar{\rho} = \spadesuit/R$):

$$u^2(\bar{\rho}, \vartheta, \varphi) = R^2\bar{\rho}^2\dot{\vartheta}^2\left[1 + \left(\frac{\spadesuit'}{\spadesuit}\right)^2\right] + \frac{\eta_e^2\left[\psi(\rho, \vartheta) - \psi_o\right]^2}{4\pi^2\spadesuit^2 \sin^2 \vartheta} = u_i^2(\vartheta_i) + 2\eta_e V(\bar{\rho}, \vartheta) \tag{B13}$$

Equation (B13) may be normalized in terms of the dc electron energy $u_o^2 = 2\eta V_o$. Dividing both sides of equation (B13) by $u_o^2 = 2\eta V_o$ yields

$$\frac{u^2(\bar{\rho}, \vartheta, \varphi)}{u_o^2} = \frac{u_i^2(\vartheta_i)}{u_o^2} + \frac{V(\bar{\rho}, \vartheta)}{V_o} = \epsilon_i(\vartheta_i) + \frac{V(\bar{\rho}, \vartheta)}{V_o} \tag{B14}$$

or

$$\frac{R^2\bar{\rho}^2\dot{\vartheta}^2\left[1+\left(\frac{\rho'}{\rho}\right)^2\right]}{2\eta_e V_o} = \epsilon_i(\vartheta_i) + \frac{V(\bar{\rho},\vartheta)}{V_o} - \frac{\eta_e^2\left[\nu(\bar{\rho},\vartheta) - \psi_c\right]^2}{(4\pi^2)(2\eta_e V_o)(R^2\bar{\rho}^2\sin^2\vartheta)} \tag{B15}$$

Solving equation (B15) for $\dot{\vartheta}^2$ yields

$$\dot{\vartheta}^2 = \frac{2\eta_e V_o\left[\epsilon_i(\vartheta_i) + \frac{V(\bar{\rho},\vartheta)}{V_o}\right]}{R^2\rho^2\left[1+\left(\frac{\rho'}{\rho}\right)^2\right]} - \frac{\eta_e^2\left[\nu(\bar{\rho},\vartheta) - \psi_c\right]^2}{4\pi^2R^4\bar{\rho}(4\sin^2\vartheta)\left[1+\left(\frac{\rho'}{\rho}\right)^2\right]} \tag{B16}$$

It is possible now to eliminate the time from equation (B7a) such as to yield a time-free trajectory $\bar{\rho} = \bar{\rho}(\vartheta, \vartheta_i, \epsilon_i, \bar{\rho}'_i)$; $\rho_i(\vartheta_i)$ and $\bar{\rho}'_i(\vartheta_i)$ being the initial values at the beginning of integration for a given initial energy class ϵ_i. The validity of the "time-free" trajectories has been discussed in the section Initial Beam Conditions. Here, we wish to repeat that this assumption holds exactly only at a given phase of entry (time) of the radiofrequency field into the collector and represents a good approximation at the mean phase of entry of the decelerated electron bunch. Since, in well-designed tubes, the electron bunch accounts for about 80 percent of all electrons during a full radiofrequency cycle, our assumption describes a good average. With this understanding in mind we write $\dot{\rho} = \rho'\dot{\vartheta}$; $\ddot{\rho} = \rho''\dot{\vartheta}^2 + \rho'\ddot{\vartheta}$; $\rho' = \partial\rho/\partial\vartheta$ and substitute this into equations (B7a) and (B7b) to obtain

$$\bar{\rho}''\dot{\vartheta}^2 + \bar{\rho}'\ddot{\vartheta} - \bar{\rho}(\sin^2\vartheta)\dot{\varphi}^2 - \bar{\rho}\dot{\vartheta}^2 - \frac{\eta_e}{R^2}\frac{\partial V}{\partial\bar{\rho}} - \frac{\eta}{R}(\sin\vartheta)A_\varphi\dot{\varphi} - \frac{\eta}{R}\bar{\rho}(\sin\vartheta)\dot{\varphi}\frac{\partial A_\varphi}{\partial\bar{\rho}} = 0 \tag{B17}$$

$$\ddot{\vartheta} = -2\frac{\bar{\rho}'}{\bar{\rho}}\dot{\vartheta}^2 + \sin\vartheta(\cos\vartheta)\dot{\varphi}^2 + \frac{\eta_e}{\bar{\rho}^2R^2}\frac{\partial V}{\partial\vartheta} + \frac{\eta_e}{\bar{\rho}R}(\cos\vartheta)\dot{\varphi}A_\varphi + \frac{\eta_e}{\bar{\rho}R}\sin\vartheta\dot{\varphi}\frac{\partial A_\varphi}{\partial\vartheta} \tag{B18}$$

After substituting $\ddot{\vartheta}$ from equation (B18) and $\dot{\vartheta}^2$ from equation (B16) into equation (B17), the latter can be solved for $\bar{\rho} = \bar{\rho}(\vartheta)$ providing that $\bar{\rho}_i(\vartheta_i)$ and $\bar{\rho}'_i(\vartheta_i)$ are known for each single electron.

APPENDIX C

DERIVATION OF CONTINUITY EQUATION

We derive now an expression for the charge density in the collector. To make the problem amenable to numerical treatments, which we wish to limit to a reasonable effort, we invoke the following assumptions made earlier in this report (see section Initial Beam Conditions).

(1) The time dependence is dropped; that is, all electrons entering the collector during the interval of one radiofrequency cycle are thought of as entering at the same time (steady-state solution).

(2) The current density across the beam is constant.

(3) The axial velocity (energy) distribution is given quantitatively by large signal computer results or other accurate methods.

(4) The angles of injection α_i are zero on the axis and proportional to the radius of injection away from the axis.

(5) Compared to the size of the collector, the entrance area in the injection plane is very small (but not zero); that is, it can be regarded as approaching a point source.

The last assumption is very important for achieving a numerical solution compatible with present knowledge and an acceptable computer volume. It is that after a distance large compared to hole radius a but small compared to collector radius $R >> a$, the electron trajectories are, in essence, independent of their initial radial position (point source) and, therefore, are determined only by the magnitude and direction of the initial velocity vector. Thus, it is permissible to locate the slowest electrons at the edge of the hole and the faster ones more toward the center as long as their population and direction are kept in accord with the actual distribution function.

To solve the continuity equation we can use either its differential, steady-state form

$$\nabla \cdot (\rho_e \cdot \bar{u}) = 0 \tag{C1}$$

or its integral (valid generally also for nonstationary flows)

$$\rho_e(x_i) \cdot J = \rho_0(a_i) \qquad i = 1, 2, 3 \tag{C2}$$

where

$$J = \frac{\partial(x_1, x_2, x_3)}{\partial(a_1, a_2, a_3)} \tag{C3}$$

is the Jacobian of the spaces d(x) and d(a) occupied by the compressible electron fluid at the times t and t = 0, respectively. To be valid in the general case of motion of the electron fluid, including overtaking and crossovers (nonlaminarity), the integration should be performed "at large" in the Lagrangian fashion by tracking all electrons from their startup volume element d(a) at the time t = 0 to their respective position d(x) at t = t. We shall solve the problem for two different cases. In the first case we assume either that the beam has been refocused or that its radial velocities are so small, even without refocusing, that it may be considered essentially parallel, say of less than 5^{o} angular spread.

Beam Almost Parallel

Consider now figure 11(a) showing a tube of electron fluid injected at the hole between S_1 and S_2, at distances r_i and $r_i + dr_i$, respectively, away from the axis 0 - 0'. Since the total dc current into the collector is continuous and the current

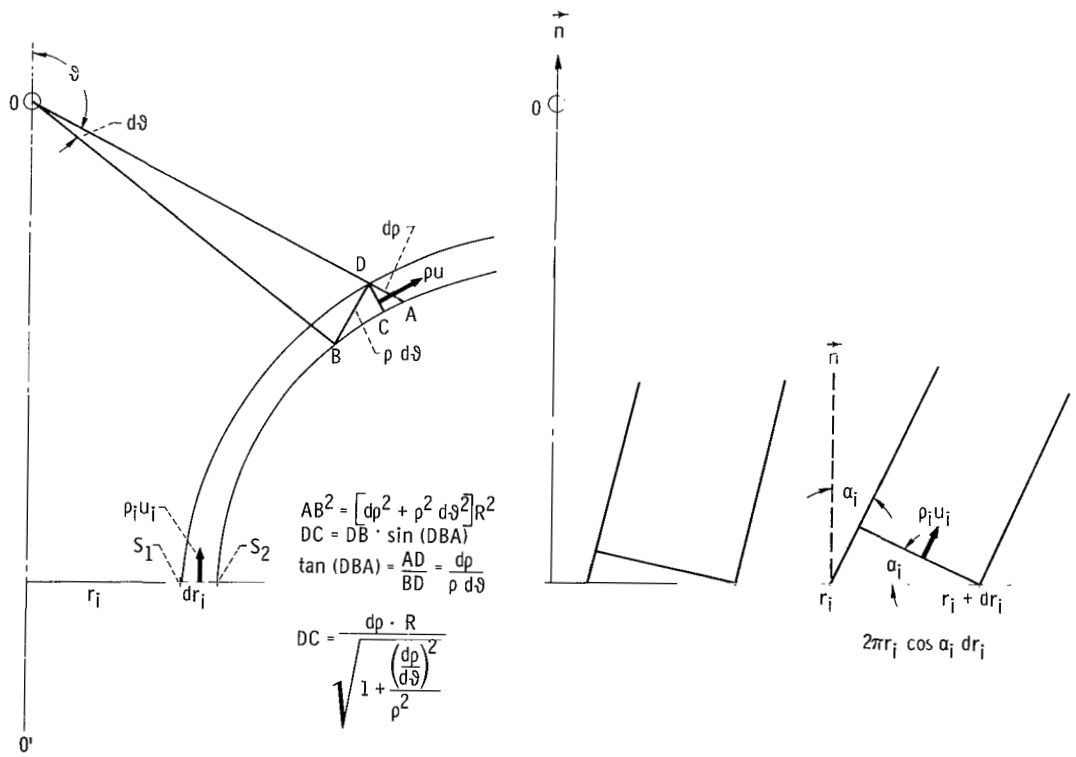

(a) Nearly parallel beam.

(b) Diverging beam

Figure 11. - Derivation of continuity equation.

density J_o is constant across the beam, the current element dI_o crossing between S_1 and S_2 is

$$dI_o = 2\pi J_o r_i \, dr_i \tag{C4}$$

To compute the trajectories of the electrons which started between S_1 and S_2 at $t = 0$, we need to know their initial velocity vector $\vec{u}_i$ and also the injection radius as a function of energy. Suppose now that the axial energy distribution function is given by $N(\epsilon)$:

$$\int_{\epsilon_{min}}^{\epsilon_{max}} dN(\epsilon) = N(\epsilon_{max}) - N(\epsilon_{min}) = -N(\epsilon_{min}) = -1 \tag{C5}$$

because $N(\epsilon_{max}) = 0$. In equation (C5), $N(\epsilon)$ determines the fraction of electrons with energies larger than ϵ. Since the distribution is non-Maxwellian, ϵ_{max} is finite and, in most cases, $\epsilon_{max} \leq 2$; ϵ_{min} is slightly larger than zero; and most of the electrons are grouped around $\epsilon \approx 0.3$ to 0.7.

We return now to equation (C4). In light of what was said before regarding the distribution of velocities, let the area $dA(\epsilon_i)$ in the injection plane occupied by electrons in the energy interval between $\epsilon_i + d\epsilon_i$ be

$$dA(\epsilon_i) = 2\pi r_i(\epsilon_i) \, dr_i(\epsilon_i) \tag{C6}$$

On the other hand, the number of electrons per second (current) in this energy group is $dI(\epsilon_i)$. This gives a current density

$$\frac{dI(\epsilon_i)}{2\pi r_i(\epsilon_i) \, dr_i(\epsilon_i)} = J_o = \text{Constant} \tag{C7}$$

Equation (C7) permits the calculation of $r_i(\epsilon_i)$

$$2\pi \int_{r=0}^{r=r_i} r(\epsilon_i) \, dr(\epsilon_i) = \frac{1}{J_o} \int_{\epsilon_{min}}^{\epsilon_i} dI(\epsilon_i) = \frac{N(\epsilon_i) - 1}{J_o} = \pi r_i^2(\epsilon_i)$$

After a flight time t, the infinitesimal volume element $dA_i \times dh$ has moved along the

trajectory to CD in figure 11(a). Let the particle velocity at CD in the direction normal to CD be $u_\perp$, then the height of the volume element at AD is $dh \cdot u_\perp/u_i$. From figure 11(a) it can be found that

$$CD = \frac{\bar{\rho}\, d\bar{\rho}}{\left[\bar{\rho}^2 + (\bar{\rho}')^2\right]^{1/2}} R \tag{C8}$$

Thus the initial volume element $dA_i \times dh$ has changed into

$$2\pi R^2 \frac{\bar{\rho}\, d\bar{\rho} \sin\vartheta}{\left[\bar{\rho}^2 + (\bar{\rho}')^2\right]^{1/2}} dh \frac{u_\perp}{u_i} \tag{C9}$$

From equation (C2) we get, since the volume element as it moves along the trajectory contains an unchanging number of electrons:

$$dA_i\, dh\rho_i = \frac{2\pi R^2 \bar{\rho}\, d\rho \sin\vartheta}{\left[\bar{\rho}^2 + (\bar{\rho}')^2\right]^{1/2}} dz \frac{u_\perp}{u_i} \rho_e \tag{C10}$$

$$\rho_e(\bar{\rho}, \vartheta) = (\rho_i u_i) \cdot \frac{r_i(\epsilon_i)\, dr_i(\epsilon_i)}{u_\perp(\bar{\rho},\vartheta)} \frac{\sqrt{\bar{\rho}^2 + (\bar{\rho}')^2}}{R^2 \bar{\rho}\, d\bar{\rho} \sin\vartheta} = \frac{J_o \dfrac{r_i(\epsilon_i)}{\bar{\rho}} \dfrac{\partial r_i}{\partial \bar{\rho}}}{R^2 u_\perp(\bar{\rho},\vartheta)} \frac{\sqrt{\bar{\rho}^2 + (\bar{\rho}')^2}}{\sin\vartheta} \tag{C11}$$

From equation (B14) we have

$$u^2(\bar{\rho}, \vartheta) = 2\eta_e V_o \left[\epsilon_i(\vartheta_i) + \frac{V(\bar{\rho}, \vartheta)}{V_o}\right] \tag{B14}$$

However, from equation (B15) the velocity component $u_\perp$ normal to CD is

$$u_\perp^2 (\bar{\rho}, \vartheta) = 2\eta_e V_o \left\{ \epsilon(\vartheta_i) + \frac{V(\bar{\rho}, \vartheta)}{V_o} - \frac{\eta_e^2 \left[\psi(\bar{\rho}, \vartheta) - \psi_o\right]^2}{(4\pi^2)(2\eta_e V_o) R^2 \bar{\rho}^2 \sin^2\vartheta} \right\} \tag{B15}$$

because the rotation in the φ-direction does not contribute to the outflow of the electrons.

It is obvious that the Jacobian (eq. (C3)) of our problem has been derived from geometrical considerations, rather than formally from the Jacobian determinant. As dis-

cussed earlier, for the solution (eq. (C11)) to be valid generally for nonlaminar flows and non-steady-state conditions, the trajectory integration must be carried out for a sufficient number of initial times and all trajectories must be computed continuously. If crossovers and overtaking occur; that is, if streamline tubes which start from different initial segments of the injection plane or streamlines which take off from the same initial segment but at a different time t_o are found at the same time t in the same volume element, all particles at crossover points must be added to account for proper space-charge density ρ_e. From this fact, the numerical complexity of integrating nonlaminar flow is apparent. With this remark we proceed now to discuss nonparallel, multivelocity streams.

Diverging, Multivelocity Beam

To treat this more complicated case, we need a two-dimensional distribution function which relates energy and direction. From assumption 4 (at the beginning of this appendix), which is quite accurate for confined-flow beams emerging through an aperture in a magnetic shield, we have for the angle $\alpha_i (\alpha_i \leq 15^o)$

$$\tan \alpha_i \approx \alpha_i = \frac{u_r}{u_z} = c r_i \tag{C12}$$

The constant c is determined from

$$\tan \alpha_{i,\max} = c r_{i,\max} \tag{C13}$$

$$c = \frac{\tan \alpha_{i,\max}}{r_{i,\max}}$$

Consider now a small element of the injection area (see fig. 11(b))

$$dA_i = 2\pi r_i \, dr_i \tag{C14}$$

The current injected through this area $dI(r_i)$ contains electrons covering the entire energy spectrum $\epsilon_{min} \leq \epsilon_i \leq \epsilon_{max}$ but of the same angular direction $\tan \alpha_i = c r_i$. Thus

$$dI(r_i) = \overrightarrow{J_o} \cdot \overrightarrow{dA_i} \tag{C15}$$

The fraction of electrons per second entering between r_i and $r_i + dr_i$ and with an energy between ϵ_i and $\epsilon_i + d\epsilon_i$ is, therefore

$$dI(r_i) = \frac{dN}{d\epsilon_i} d\epsilon_i = J_o(2\pi r_i)\frac{dN}{d\epsilon_i} (\cos \alpha)\, dr_i\, d\epsilon_i \tag{C16}$$

The initial volume element containing a certain amount of fluid (electrons) of a given velocity class u_{ij} is

$$2\pi r_i\, dr_i \cos \alpha_i\, dh \tag{C17}$$

The charge density ρ_{ij} associated with the velocity class u_{ij} times the volume element (eq. (C17)) gives a charge

$$2\pi r_i(\cos \alpha_i)\rho_{ij}\, dh\, dr_i \tag{C18}$$

As this charge moves along the trajectory, the volume element occupied by it will be

$$2\pi R^2 \frac{\bar{\rho}\, d\bar{\rho} \sin \vartheta}{\sqrt{\bar{\rho}^2 + \left(\frac{\partial \bar{\rho}}{\partial \vartheta}\right)^2}} \frac{u_{\perp ij}(\bar{\rho}, \vartheta)}{u_{ij}} dh \tag{C19}$$

and the charge density in it is $\rho_{eij}(\bar{\rho}, \vartheta)$. Thus, from conservation of charge we have

$$\rho_{eij}(\bar{\rho}, \vartheta) = \frac{\frac{r_i}{\bar{\rho}} \frac{\partial r_i}{\partial \bar{\rho}} \sqrt{\bar{\rho}^2 + \left(\frac{\partial \bar{\rho}}{\partial \vartheta}\right)^2}}{(\sin \vartheta) R^2 u_{ij\perp}(\bar{\rho}, \vartheta)} \cos \alpha_i(\rho_{ij} u_{ij}) \tag{C20}$$

This is the space-charge density at the location $\bar{\rho}, \vartheta$ due to electrons injected at $r = r_i$ with an angle α_i and within an energy class ϵ_j. Because the motion is nonlaminar, there may be contributions to $\rho_{eij}(\bar{\rho}, \vartheta)$ stemming from electrons which have started at difference initial locations r_i and with different energies ϵ_j. For a steady-state motion

the crossovers will occur at certain time-independent locations. Thus, the total $\rho_e(\bar{\rho}, \vartheta)$ is obtained, whenever crossovers occur, from the summation

$$\rho_e(\bar{\rho}, \vartheta) = \sum_{r_i} \sum_{u_j} \rho_{eij}(\bar{\rho}, \vartheta) \tag{C21}$$

In equation (C20) the product $\cos \alpha_i(\rho_{ij} u_{ij})$ represents the component J_{ij} of the current density due to the velocity class j. Integration over all velocity classes results in the current density $J_{oi} \equiv J_o$, which is, by assumption, independent of location r_i and, therefore, constant over the injection hole.

Because trajectories are not known in advance, a closed-form solution is not feasible. Also, due to the interdependence of trajectories and space-charge densities, a relaxation-type solution is required. The reduction of space-charge density, which is desirable for reasons described earlier (in the section Space-Charge Effects), substantially speeds up the convergence.

APPENDIX D

SOLUTION OF THE MAGNETIC-BOUNDARY-VALUE PROBLEM

Expression for Component $A_\varphi(r,z)$ of Magnetic Vector Potential in Cylindrical, Axisymmetric Coordinates (ref. 6)

$$A_\varphi(r,z) = \sum_{n=0}^{\infty} \frac{(-1)^n}{n!(n+1)!} \frac{\partial^{2n} B(0,z)}{\partial z^{2n}} \left(\frac{r}{2}\right)^{(2n+1)}$$

$$= B(0,z)\frac{r}{2} - \frac{1}{1!2!} B^{(2)}(0,z)\frac{r^3}{2^3} + \frac{1}{2!3!} B^{(4)}(0,z)\frac{r^5}{2^5} - \frac{1}{3!4!} B^{(6)}(0,z)\frac{r^7}{2^7} - + \ldots \quad \text{(D1)}$$

Expression for Leakage of Magnetic Induction Density Through a Circular Aperture in a Shielding, Infinite Plane Sheet

Let the location of the plane in a r, φ, z coordinate system be at z = 0, the plane extending to infinity in every direction normal to the z-axis. Let the sheet be made of a magnetic material with a $\mu = \infty$ and a B at saturation $B_{sat} = \infty$. Let the B to the left of z = 0, that is, at negative values of z, approach a constant value B_o such that $B(0, -\infty) = B_o$. To the right of the shielding plane, $B(0,z)$ decays to zero such that $B(0, +\infty) = 0$. The scalar magnetic potential V_m from which the required leakage field can be derived as $B = -\text{grad } V_m$ is (ref. 6, ch. 5.272):

$$V_m = aB_o\xi\left[(-\zeta) + \frac{1}{\pi}\zeta \cot^{-1}(-\zeta) + \frac{1}{\pi}\right] \quad \text{(D2)}$$

In equation (D2), ξ and ζ are the coordinates of oblate spheroids. The third coordinate is, of course, the angle φ, same as in cylindrical coordinates.

The coordinates ξ and ζ are related to circular cylindrical coordinates r and z through the relations

$$z = a\xi\zeta \quad \text{(D3a)}$$

$$r = a\left[1 + \zeta^2)(1 - \xi^2\right]^{1/2} \tag{D3b}$$

The range of ξ and ζ is $0 \leq \xi \leq +1$ and $-\infty < \zeta < +\infty$; also, sign ζ = sign z. On the sheet, $\xi = 0$; inside the hole in the plane, $\zeta = 0$; at the edge of the hole $r = a$, $z = 0$, both ξ and ζ are zero. Equations (D3) can be solved for ζ and ξ:

$$a\zeta = \sqrt{r^2 - a^2 + z^2 + \sqrt{\left(r^2 + z^2\right)^2 + a^2(a^2 - 2r^2 + 2z^2)}} \tag{D4}$$

$$\xi = \frac{z}{\sqrt{r^2 - a^2 + z^2 + \sqrt{\left(r^2 + z^2\right)^2 + a^2(a^2 - 2r^2 + 2z^2}}} \tag{D5}$$

Notice that inside the hole in the plane $z = 0$, $\xi \neq 0$. The values ξ in the hole may be obtained from equation (D3b) by setting $\zeta = 0$ and $r = a(1 - \xi^2)^{1/2}$. At $r = z = 0$, it follows $\xi = 1$ from either equation (D3b) or equation (D5) as the limit of ξ for $z \to 0$ $(r = 0)$. The transformation from cylindrical coordinates r, z into spherical coordinates ρ, ϑ may be accomplished with the use of equations (B2) and (B3):

$$r = \rho \sin \vartheta \tag{B2}$$

$$z = R + \rho \cos \vartheta \tag{B3}$$

Substituting first equations (B2) and (B3) for r and z into equations (D4) and (D5) and then the values $\zeta = \zeta(\rho, \vartheta)$ and $\xi = \xi(\rho, \vartheta)$ into equation (D2), an expression $V_m = V_m(\rho, \vartheta)$ is obtained, from which we get

$$B_\rho(\rho, \vartheta) = -\frac{\partial V_m}{\partial \rho} \tag{D6}$$

$$B_\vartheta(\rho, \vartheta) = -\frac{1}{\rho}\frac{\partial V_m}{\partial \vartheta} \tag{D7}$$

This procedure is straightforward. Although the resulting equations can be obtained in closed analytical expressions, they are very cumbersome and are more easily produced through numerical analysis.

Equation (D2) and the field components (eqs. (D6) and (D7)) are valid everywhere. Inside the hole $r \leq a$, a series solution for $A_\varphi(r,z)$ may be obtained from equations (D1) and (D2). Now on the axis $r = 0$, $\xi = 1$ and $z = a\zeta$. Thus, equation (D2) simplifies to

$$V_m(0,z) = aB_o\left\{\left(-\frac{z}{a}\right) + \frac{1}{\pi}\left[\frac{z}{a}\cot^{-1}\left(-\frac{z}{a}\right)\right] + \frac{1}{\pi}\right\} \tag{D8}$$

and

$$B_z(0,z) = -\frac{\partial V_m(0,z)}{\partial z} = B_o\left[1 - \frac{1}{\pi}\cot^{-1}\left(-\frac{z}{a}\right)\right] - \frac{B_o}{\pi}\frac{\frac{z}{a}}{1+\left(\frac{z}{a}\right)^2} \tag{D9}$$

Notice that $B_z(0,0) = \frac{1}{2}B_o$, which is the same as the field of a long homogeneously wound solenoid at its end.

Since $B = \text{curl } A$, we get

$$B_z(r,z) = \frac{A_\varphi(r,z)}{r} + \frac{\partial A_\varphi(r,z)}{\partial r} \tag{D10}$$

$$B_r(r,z) = -\frac{\partial A_\varphi(r,z)}{\partial z} \tag{D11}$$

After $B_z(0,z)$ (eq. (D9)) has been substituted into equation (D1), expressions for $B_z(r,z)$ and $B_r(r,z)$ are obtained from equations (D10) and (D11). The first six derivatives of $B_z(0,z)$ are listed below. Using $\mathcal{z}$ as an abbreviation for z/a,

$$B_z^{(1)}(0,z) = -\frac{2B_o}{\pi a}\frac{1}{(1+\mathcal{z}^2)^2} \tag{D12}$$

$$B_z^{(2)}(0,z) = +\frac{8B_o}{\pi a^2}\frac{\mathcal{z}}{(1+\mathcal{z}^2)^3} \tag{D13}$$

$$B_z^{(3)}(0,z) = +\frac{8B_o}{\pi a^3}\frac{1-5\mathcal{z}^2}{(1+\mathcal{z}^2)^4} \tag{D14}$$

$$B_z^{(4)}(0,z) = -\frac{48B_o}{\pi a^4}\mathcal{z}\frac{3-5\mathcal{z}^2}{(1+\mathcal{z}^2)^5} \tag{D15}$$

$$B_z^{(5)}(0,z) = -\frac{48B_o}{\pi a^5}\,\frac{3 - 42\mathfrak{z}^2 + 35\mathfrak{z}^4}{(1+\mathfrak{z}^2)^6} \tag{D16}$$

$$B_z^{(6)}(0,z) = +\frac{1920}{\pi a^6}\,B_o\mathfrak{z}\,\frac{3 - 14\mathfrak{z}^2 + 7\mathfrak{z}^4}{(1+\mathfrak{z}^2)^7} \tag{D17}$$

From equations (D12) to (D17) and (D1),

$$\frac{A_\varphi(r,z)}{B_o} \frac{r}{2}\left[1 - \frac{1}{\pi}\cot^{-1}(-\mathfrak{z}) - \frac{1}{\pi}\,\frac{\mathfrak{z}}{1+\mathfrak{z}^2}\right] - \frac{r^3}{2\pi a^2}\,\frac{\mathfrak{z}}{(1+\mathfrak{z}^2)^3}$$

$$- \frac{r^5}{8\pi a^4}\,\mathfrak{z}\,\frac{3 - 5\mathfrak{z}^2}{(1+\mathfrak{z}^2)^5} - \frac{5r^7}{48\pi a^6}\,\mathfrak{z}\,\frac{3 - 14\mathfrak{z}^2 + 7\mathfrak{z}^4}{(1+\mathfrak{z}^2)^7} + - \ldots \tag{D18}$$

For the equations of motion in appendix B this expression for $A_\varphi(r,z)$ must be transformed into spherical coordinates ρ and ϑ as before. Notice that $z = 0$, $r = 0$ (center of the aperture in fig. 10) does not coincide with $\mathfrak{z} = R\rho = 0$ (center of the sphere and origin of the spherical coordinate system).

From equations (D18), (B2), and (B3), we get for $A_\varphi = A_\varphi(\rho, \vartheta)$:

(D19)

APPENDIX E

COMPUTATION OF RESULTS

The electron trajectories and equations associated with their derivations were computed on a high-speed digital computer. The details of the computations are not given here, but will be dealt with in a separate publication. Here we state the chosen approach only.

The solution of the boundary-value problem was accomplished in part with the Green's function series on the sphere and in part with the finite difference method along the spike since working with elliptical harmonics proved more involved than a direct way of forcing the boundary value along the spike. For the solution concerning conical boundaries, noninteger-order ν Legendre polynomials $P_\nu^m(-\cos\vartheta)$ were needed which are zero along the cone ($\cos\vartheta$ = Constant) or hyperboloid (ξ_c = Constant) tangential to the cone. Since the polynomials $P_\nu^m(z)$ may be expressed by hypergeometric functions which contain the orders ν and m as parameters, the latter may be computed from suitable hypergeometric series $F(m - \nu,\ m + \nu + 1,\ m + 1,\ \sin^2 \vartheta/2)$. See, for example, references 7 to 9, from which $P_\nu^m(\cos\vartheta)$ is obtained as

$$P_\nu^m(\cos\vartheta) = \frac{(-1)^m(\nu + m)!\ \sin^m\vartheta}{2^m(\nu - m)!\,m!}\ F\left(m - \nu,\ m + \nu + 1,\ m + 1,\ \sin^2\frac{\vartheta}{2}\right)$$

Here the unknown is the order ν which, for a given value of m and for $\cos\vartheta$ = Constant, makes $P_\nu^m(\cos\vartheta) = 0$.

A particularly difficult computation problem is posed by the requirement to solve the Poisson equation for current densities approaching 100 amperes per square centimeter at the injection hole. As many as six iterations were necessary for achieving a convergent solution. Since with every single iteration the results tend to "swing out" to far off, the application of the predictor-corrector method proved necessary and sufficient for speeding up and obtaining convergence. Variable-size mesh was used because of the congestion of trajectories in the vicinity of the injection hole. The computational step in computing the "high-space-charge" cases of trajectories was 0.001R and 0.001° in ϑ as minimum and 0.01R and 0.1° ϑ as maximum.

APPENDIX F

SYMBOLS

$A(r,z)$	vector potential
A_{nm}, B_{nm}, C_{nm}	expansion coefficients
a	radius of hole
B	magnetic field density, Wb/m^2
b, c	minor and major axis of spheroids of revolution
e	electron charge, Asec
G	Green's function
h	height
h_1, h_2, h_3	metric coefficients
I	current
i_1	normalized radiofrequency current
J	Jacobian determinant
J_o	current density, A/cm^2
j	$\sqrt{-1}$
k	coupling factor; summation number
L*	generalized Lagrangian
m	upper order of Legendre polynomials
m_e	electron mass
N	normalized distribution function
n, ν	lower order of Legendre polynomials
$\bar{n}$	normal direction pointing out of integration area
P	power, W
$P_n^m()$	Legendre functions of first kind
$Q_n^m()$	Legendre functions of second kind
q	electric charge, A · sec
R	radius of sphere
r	distance from axis
r, φ, z	cylindrical coordinates
$\mathscr{r}$, ϑ, φ	spherical coordinates
S	surface boundary
t	time, sec
u	velocity, m/sec
$\mathscr{V}$	volume enclosed by surface S
V	voltage
v_1	normalized radiofrequency voltage
$\mathscr{z}$	normalized length, z/a
α_i	injection angle
δ_m^o	Kronecker delta
ϵ	normalized energy
ϵ_o	dielectric constant, $8.86\times10^{-11}\ C^2/N/m^2$

$H(\eta)$, $\Xi(\xi)$, $\Phi(\varphi)$	factors in product solution of Laplace equations in prolate spheroidal coordinates
ϑ	cone angle
μ	cos ϑ
ξ, ζ, φ	oblate spheroidal coordinates
ξ, η, φ	prolate spheroidal coordinates
$\bar{\rho}$	normalized radius, r/R
ρ_e	volume charge density, $Asec/m^3$
η	efficiency
$\eta_e = e/m_e$	electron charge to mass ratio
σ	surface-charge density, $Asec/m^2$
ψ	magnetic flux, Wb

Subscripts:

B	Brillouin
c	collector
ct	circuit
e	electron, electronic
i	initial injection plane
l	lens
m	magnetic
o	source or dc
ov	overall
RF	radiofrequency
r	radial
sat	saturation
si	superimposed
t	tube

Superscripts:

$\cdot$	total derivative with respect to time, d/dt
$'$	partial derivative with respect to space, $\partial/\partial s$

REFERENCES

1. Wolkstein, H. J.: Effect of Collector Potential on the Efficiency of Traveling-Wave Tubes. RCA Rev., vol. 19, no. 2, June 1958, pp. 259-282.

2. Sterzer, F.: Improvement of Traveling-Wave Tube Efficiency through Collector Potential Depression. IRE Trans. on Electron Devices, vol. ED-5, no. 4, Oct. 1958, pp. 300-305.

3. Sauseng, O. G.: Applied Research on Efficiency Improvement in O-Type Traveling-Wave Tubes. Hughes Aircraft Co. (RADC TR-67-259, DDC No. AD-818085), Apr. 1967.

4. Sauseng, O. G.; Basilulis, A.; and Tammaru, I.: Analytical Study Program to Develop the Theoretical Design of Traveling-Wave Tubes. Rep. HAC-EDD-W-2646, Hughes Aircraft Co. (NASA CR-72450), Oct. 31, 1968.

5. Branch, G. M.; and Mihran, T. G.: Analytical Designs of a Space-Borne Magnetically-Focused Klystron Amplifier. General Electric Co. (NASA CR-72461), Oct. 25, 1968, pp. 109-119.

6. Smythe, William R.: Static and Dynamic Electricity. Second ed., McGraw-Hill Book Co., Inc., 1950.

7. Magnus, Wilhelm; and Oberhettinger, Fritz: Formulas and Theorems for the Special Functions of Mathematical Physics. Chelsea Publ. Co., 1949.

8. Abramowitz, Milton; and Stegun, Irene A., eds.: Handbook of Mathematical Functions with Formulas, Graphs, and Mathematical Tables. Appl. Math. Ser. 55, National Bureau of Standards, 1964, Chs. 8 and 15.

9. Schelkunoff, S. A.: Applied Mathematics for Engineers and Scientists. Second ed., D. Van Nostrand Co., 1965, p. 429.

"The aeronautical and space activities of the United States shall be conducted so as to contribute . . . to the expansion of human knowledge of phenomena in the atmosphere and space. The Administration shall provide for the widest practicable and appropriate dissemination of information concerning its activities and the results thereof."

—NATIONAL AERONAUTICS AND SPACE ACT OF 1958

NASA SCIENTIFIC AND TECHNICAL PUBLICATIONS

TECHNICAL REPORTS: Scientific and technical information considered important, complete, and a lasting contribution to existing knowledge.

TECHNICAL NOTES: Information less broad in scope but nevertheless of importance as a contribution to existing knowledge.

TECHNICAL MEMORANDUMS: Information receiving limited distribution because of preliminary data, security classification, or other reasons.

CONTRACTOR REPORTS: Scientific and technical information generated under a NASA contract or grant and considered an important contribution to existing knowledge.

TECHNICAL TRANSLATIONS: Information published in a foreign language considered to merit NASA distribution in English.

SPECIAL PUBLICATIONS: Information derived from or of value to NASA activities. Publications include conference proceedings, monographs, data compilations, handbooks, sourcebooks, and special bibliographies.

TECHNOLOGY UTILIZATION PUBLICATIONS: Information on technology used by NASA that may be of particular interest in commercial and other non-aerospace applications. Publications include Tech Briefs, Technology Utilization Reports and Technology Surveys.

Details on the availability of these publications may be obtained from:

SCIENTIFIC AND TECHNICAL INFORMATION OFFICE

NATIONAL AERONAUTICS AND SPACE ADMINISTRATION

Washington, D.C. 20546